Chapter 4
The Transfer Matrix Method in Acoustics

Modelling One-Dimensional Acoustic Systems, Phononic Crystals and Acoustic Metamaterials

Noé Jiménez, Jean-Philippe Groby, and Vicent Romero-García

Abstract The transfer matrix method is a simple but powerful analytical tool used to model acoustic wave propagation in a wide range of one-dimensional problems. In this chapter, we present the method and summarize the most common building blocks encountered in one-dimensional acoustic systems. These include layers of fluids and porous media, ducts and waveguides of different geometries where thermoviscous losses can be accounted for, locally reacting elements such as Helmholtz or quarter-wavelength resonators, viscoelastic plates and membranes, micro-perforated panels or vibrating walls. Several examples are provided, including a multi-layered porous structure for room acoustics, the transmission problem of a double-leaf wall for building acoustics, and the analysis of the dispersion relations of acoustic waves in periodic media and metamaterials using locally resonant elements. Various one-dimensional wave-motion phenomena can be studied using the generalized framework provided by the transfer matrix method such as reflection, transmission, absorption, attenuation and dispersion, as illustrated in the examples.

4.1 Introduction

Many acoustic problems of practical interest can be reduced to one-dimensional ones under the hypothesis of plane-wave propagation. Analytical solutions can thus

N. Jiménez (✉)
Instituto de Instrumentación para Imagen Molecular, Universitat Politècnica de València, CSIC, Camino de Vera S/N, València, Spain
e-mail: nojigon@upv.es

J.-P. Groby · V. Romero-García
Laboratoire d'Acoustique de l'Université du Mans, UMR CNRS 6613, Le Mans Université, Avenue Olivier Messiaen, 72085 Le Mans, France
e-mail: jean-philippe.groby@univ-lemans.fr

V. Romero-García
e-mail: vicente.romero@univ-lemans.fr

N. Jiménez et al. (eds.), *Acoustic Waves in Periodic Structures, Metamaterials, and Porous Media*, Topics in Applied Physics 143,
https://doi.org/10.1007/978-3-030-84300-7_4

be obtained under this hypothesis even for complex problems. Among the different analytical techniques such as modal expansions [1], plane wave expansion methods (PWE) (See Chap. 1) or multiple scattering theory (MST) (See Chap. 2), the transfer matrix method (TMM) [2] has been widely applied to study wave propagation in one-dimensional systems such as porous materials [3, 4], duct acoustics and mufflers with [5] and without flow [6], stratified solids [7] and multilayer elastic and acoustic materials for noise control [8–13], fluid mechanics [14], piezoelectric transducers [15] or acoustic holograms [16], among others. TMM is also at the heart of standard procedures to measure the properties and performance of acoustic materials [17]. The method is also widely applied in electromagnetics [18], e.g., to study multilayer optical structures [19, 20]. It can be applied in Cartesian and in other coordinate system, such as cylindrical coordinates for radially-symmetric multilayer structures [21].

The transfer matrix method has recently been used to described wave propagation in periodic structures and phononic crystals as well as to study acoustic metamaterials. Wave dispersion and acoustic properties such as reflection and transmission in multilayer phononic crystals can effectively be described by a transfer matrix approach [22]. The method can be used to derive the effective parameters of resonant structures [23] and even of hyperbolic metamaterials [24]. Thermoviscous and viscoelastic losses can also be easily included. In this way, this method has been applied to design and analyse efficient or perfect metamaterial absorbers based on quarter-wavelength resonators [25], Helmholtz resonators [26–28] or membranes and plates [29, 30].

The transfer matrix method results in fast calculations to describe complex acoustic structures, in fact, it is one of its most important advantages. It can thus be easily combined with optimization techniques that would be prohibitive using other simulation methods such as finite-difference in time-domain (FDTD) or Finite Element Methods (FEM) due to extreme computational resources and simulation times they would require.

In this chapter, we present the method and summarize the most common building blocks. We will describe the modelling of layers of fluids and porous media, ducts of different geometries possibly accounting for thermoviscous losses, locally resonant elements such as Helmholtz and quarter-wavelength resonators, viscoelastic membranes and plates, micro-perforated plates and vibrating walls. The last section, several examples will be given comprising a multilayer porous structure for room acoustics, a double-leaf wall for building acoustics, the dispersion of acoustic waves in periodic multilayer media, and the design of acoustic metamaterials using different kinds of resonators.

4.2 The Transfer Matrix Method

We start deriving the basic relations between the acoustic magnitudes evaluated at the boundaries of a layer of homogeneous acoustic material, as shown in Fig. 4.1.

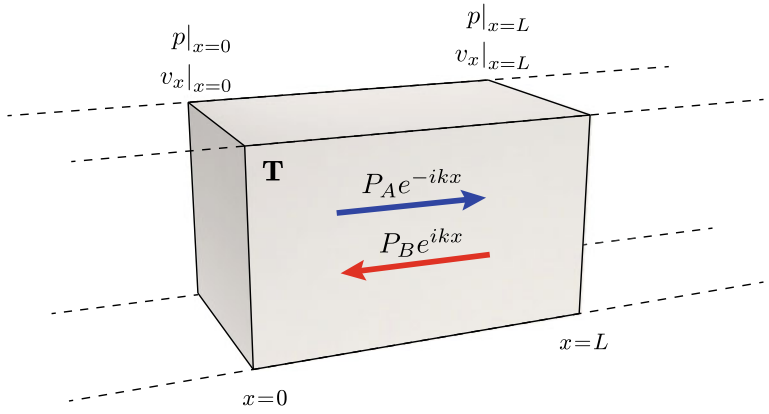

Fig. 4.1 Scheme of the acoustic material layer characterized by a transfer matrix **T**. Propagation inside the layer is modeled by counter propagating waves

Assuming that only longitudinal plane waves propagate in the layer and a temporal harmonic dependence of the type $e^{i\omega t}$, the total field inside the material is written as the superposition of two waves propagating in opposite directions as

$$p(x) = P_A e^{-ikx} + P_B e^{ikx}, \tag{4.1}$$

$$v_x(x) = \frac{P_A}{Z} e^{-ikx} - \frac{P_B}{Z} e^{ikx}, \tag{4.2}$$

where $Z = \rho c$ is the characteristic acoustic impedance, $k = \omega/c$ is the wavenumber at the angular frequency $\omega = 2\pi f$, with ρ the density and c the sound speed of the material, and the amplitudes of the two waves are given by P_A and P_B.

To evaluate these amplitudes we define the pressure and velocity at both sides of the slab. First, at $x = 0$ we obtain

$$p(x)\big|_{x=0} = P_A + P_B, \tag{4.3}$$

$$Z v_x(x)\big|_{x=0} = P_A - P_B, \tag{4.4}$$

while at $x = L$ we get

$$p(x)\big|_{x=L} = (P_A + P_B)\cos(kL) - i(P_A - P_B)\sin(kL), \tag{4.5}$$

$$v_x(x)\big|_{x=L} = \frac{P_A - P_B}{Z}\cos(kL) - i\frac{P_A - P_B}{Z}\sin(kL). \tag{4.6}$$

Then, we can relate the acoustic magnitudes at both boundaries by combining (4.3)–(4.4) with (4.5)–(4.6) via

$$p(x)\big|_{x=L} = \cos(kL)\,p(x)\big|_{x=0} - iZ\sin(kL)\,v_x(x)\big|_{x=0}, \tag{4.7}$$

$$v_x(x)\big|_{x=L} = \cos(kL)\,v_x(x)\big|_{x=0} - i\frac{1}{Z}\sin(kL)\,p(x)\big|_{x=0}. \tag{4.8}$$

Equations (4.7)–(4.8) can be expressed in a matrix form as

$$\begin{bmatrix} p \\ v_x \end{bmatrix}_{x=L} = \begin{bmatrix} \cos(kL) & -iZ\sin(kL) \\ \cos(kL) & -i\frac{1}{Z}\sin(kL) \end{bmatrix} \begin{bmatrix} p \\ v_x \end{bmatrix}_{x=0}. \tag{4.9}$$

After inversion, we retrieve the basic transfer matrix formulation of a layer of acoustic material, given by

$$\begin{bmatrix} p \\ v_x \end{bmatrix}_{x=0} = \begin{bmatrix} \cos(kL) & iZ\sin(kL) \\ i\frac{1}{Z}\sin(kL) & \cos(kL) \end{bmatrix} \begin{bmatrix} p \\ v_x \end{bmatrix}_{x=L}. \tag{4.10}$$

In this way, the acoustic magnitudes at both sides of the 1D fluid layer are related by a 2×2 matrix which only depends on the impedance and wavenumber in the material. It is interesting to note that additional elements can be introduced into the system in a simple and modular way. This allows to model complex materials and structures using a simple theoretical framework, as we will see below.

4.2.1 Total Transfer Matrix

For a given material, we can define a total transfer matrix, $\mathbf{T}$, that relates the sound pressure, p, and normal acoustic particle velocity, v_x, at the beginning, $x = 0$, and at the end of a structure, $x = L$ as

$$\begin{bmatrix} p \\ v_x \end{bmatrix}_{x=0} = \mathbf{T} \begin{bmatrix} p \\ v_x \end{bmatrix}_{x=L}, \tag{4.11}$$

therefore, the total transfer matrix $\mathbf{T}$ is a 2×2 matrix as

$$\begin{bmatrix} p \\ v_x \end{bmatrix}_{x=0} = \begin{bmatrix} T_{11} & T_{12} \\ T_{21} & T_{22} \end{bmatrix} \begin{bmatrix} p \\ v_x \end{bmatrix}_{x=L}. \tag{4.12}$$

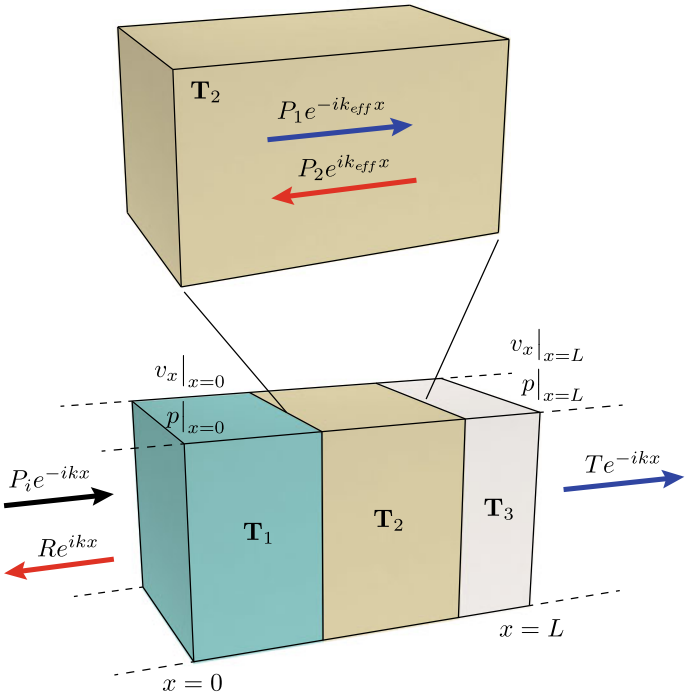

Fig. 4.2 Scheme of an acoustic structure composed by several layers of effective properties. The system is characterized by a total transfer matrix, $\mathbf{T}$, equal to the matrix product of the elements, i.e., $\mathbf{T} = \mathbf{T}_1\mathbf{T}_2\mathbf{T}_3$ in this example

When dealing with a complex structure, e.g., an arrangement of several elements as depicted in Fig. 4.2, the total transfer matrix $\mathbf{T}$ is given by the product of the transfer matrices of the N layers or elements of the system as

$$\mathbf{T} = \prod_{n=1}^{N} \mathbf{T}_n \,. \tag{4.13}$$

The continuity of pressure and normal particle velocity at each interface of the system are intrinsically satisfied. The transfer matrix of each layer or element, $\mathbf{T}_n$, is calculated according to its nature. Several basic examples will be given in Sect. 4.3 including thermoviscous fluids, fluid-saturated rigid-frame porous layers, or locally resonant elements such as elastic membranes or Helmholtz resonators.

The total transfer matrix $\mathbf{T}$ offers abundant information about the system such as:

1. *The effective parameters:* The effective impedance and wavenumber, in addition to the effective density and bulk modulus of the system in the long wavelength regime.

2. *The scattering of the system:* The reflection and transmission coefficients and, if looses are considered, the absorption coefficient.

4.2.2 Effective Parameters

In the case of a symmetric structure, the total transfer matrix **T** is symmetric and the system can be modelled as an equivalent on-dimensional fluid-like layer with complex and frequency-dependent effective parameters in the long wavelength regime. Thus, the total transfer matrix of the structure, given by (4.11), can be identified to the propagation matrix an effective material of length L, given by (4.10), as

$$\mathbf{T} = \begin{bmatrix} T_{11} & T_{12} \\ T_{21} & T_{22} \end{bmatrix} = \begin{bmatrix} \cos(k_{\text{eff}} L) & i Z_{\text{eff}} \sin(k_{\text{eff}} L) \\ i \dfrac{1}{Z_{\text{eff}}} \sin(k_{\text{eff}} L) & \cos(k_{\text{eff}} L) \end{bmatrix}, \tag{4.14}$$

where $k_{\text{eff}}(\omega)$ is the effective wavenumber and $Z_{\text{eff}}(\omega)$ is the effective characteristic impedance of the whole structure. Both effective parameters are usually complex and frequency dependent.

4.2.2.1 Effective Wavenumber

By relating the elements of (4.12) with those in (4.14) we can obtain the expression for the effective wavenumber as a function of the coefficients of the total transfer matrix

$$k_{\text{eff}} = \frac{1}{L} \cos^{-1}\left(\frac{T_{11} + T_{22}}{2}\right) + \frac{n\pi}{L}, \; n \in \mathbb{Z}. \tag{4.15}$$

It is important to note that due to the trigonometric inversion the wavenumber is warped around $-\pi < k_{\text{eff}} L < \pi$. This is very useful for periodic structures as we will see in the examples in Sect. 4.4: obtaining the wavenumber $k_{\text{eff}}(\omega)$ of a unit cell provides the dispersion relation in the irreducible Brillouin zone. It is effectively important to note that $k_{\text{eff}}(\omega)$ matches the solution of the eigenvalue problem solved for recovering the dispersion relation of any symmetric system and thus is valid whatever the frequency range considered.

4.2.2.2 Effective Characteristic Impedance

In the same way, the characteristic acoustic impedance is identified from the total transfer matrix coefficients as

$$Z_{\text{eff}} = \sqrt{\frac{T_{12}}{T_{21}}}. \tag{4.16}$$

In this case, no trigonometric inversion is used and the retrieved impedance values are measured in [Rayls] units. Nevertheless, this identification is only valid in the long wavelength regime contrary to the recovery of $k_{\text{eff}}(\omega)$ and special attention should thus be paid on the frequency validity regime.

4.2.2.3 Effective Density and Bulk Modulus

The dynamic mass-density, ρ_{eff}, and bulk modulus, K_{eff}, of the slab of effective material can be obtained using

$$K_{\text{eff}} = Z_{\text{eff}} \frac{\omega}{k_{\text{eff}}}, \quad \text{and} \quad \rho_{\text{eff}} = Z_{\text{eff}} \frac{k_{\text{eff}}}{\omega}, \tag{4.17}$$

where Z_{eff} is given by (4.16) and k_{eff} by (4.15) with proper unwrap of the wavenumber.

4.2.3 The Scattering Matrix

The scattering matrix, **S**, relates the amplitudes of the incoming waves to those of the outgoing waves. The total pressure at both sides of the structure, at $x = 0$ and $x = L$, is given by

$$p(x) = \begin{cases} Ae^{-ikx} + Be^{ikx} & \text{for} \quad x < 0, \\ Ce^{-ikx} + De^{ikx} & \text{for} \quad x > L, \end{cases} \tag{4.18}$$

as shown in Fig. 4.3 for a structure of length L. Thus, the relation between the amplitudes of both waves is given by the **S**-matrix as

$$\begin{bmatrix} C \\ B \end{bmatrix} = \mathbf{S} \begin{bmatrix} A \\ D \end{bmatrix} = \begin{bmatrix} T^- & R^+ \\ R^- & T^+ \end{bmatrix} \begin{bmatrix} A \\ D \end{bmatrix}, \tag{4.19}$$

where the elements of the **S**-matrix give directly the transmission (T^- and T^+) and reflection (R^- and R^+) coefficients for a system excited from each side of the structure, i.e., the superscripts $(+, -)$ denote the direction of incidence: the positive

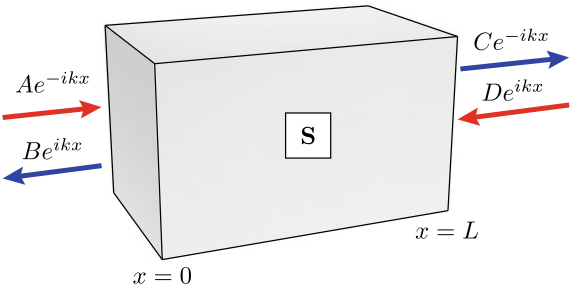

Fig. 4.3 Incoming and outgoing waves that define the scattering of the structure. The scattering matrix, **S**-matrix, completely describe the transmitted and reflected waves

and negative x-axis respectively. The **S**-matrix is widely used in wave physics to characterize and interpret the wave scattering. In the case of acoustics, the scattering matrix completely describe the transmitted and reflected waves, and when looses are included, the absorption of the system.

4.2.4 Reflection, Transmission and Absorption Coefficients

The system is usually geometrically bounded and therefore its scattering properties can be evaluated. Depending on the boundary conditions at $x = 0$ and $x = L$, we can distinguish between:

(i) *Reflection problem:* the material is located against an impervious wall. The acoustic impedance is that of the surrounding medium $Z_0 = \rho_0 c_0$ at the beginning ($x = 0$), while the rigid boundary condition is applied, i.e., $v_x = 0$, at the end of the material ($x = L$),

(ii) *Transmission problem:* the material is surrounded by a fluid on both sides. Then, the acoustic impedance is that of the surrounding media $Z_0 = \rho_0 c_0$ at $x = 0$ and $Z_L = \rho_L c_L$ at $x = L$.

For example, a layer of porous material obviously presents different reflection (and absorption) coefficient if it is located against a rigid-impervious wall (reflection problem) or if it is surrounded by air on both sides (transmission problem).

4.2.4.1 Transmission Problem

The transmission problem implies the waves impinging the structure on one side can propagate through it and be transmitted to the other side. First, (4.11) are written as

$$p(x)\big|_{x=0} = T_{11}\, p(x)\big|_{x=L} + T_{12}\, v_x(x)\big|_{x=L}\,, \tag{4.20}$$

$$v_x(x)\big|_{x=0} = T_{21}\, p(x)\big|_{x=L} + T_{22}\, v_x(x)\big|_{x=L}\,. \tag{4.21}$$

Then, assuming an incident pressure wave whose amplitude is the unity, the pressure and velocity at both sides of the structure can be defined as a function of the reflection coefficients R^+ and R^-, and the corresponding transmission coefficients, T^+ and T^-, as

$$p(x)\big|_{x=0} = 1 + R^-, \qquad p(x)\big|_{x=L} = T^- e^{ikL}, \tag{4.22}$$

$$v_x(x)\big|_{x=0} = \frac{1 - R^-}{Z_0}, \qquad v_x(x)\big|_{x=L} = \frac{T^- e^{ikL}}{Z_L}, \tag{4.23}$$

for an incident plane wave coming from $-\infty$ and propagating in the $+x$ direction, and

$$p(x)\big|_{x=0} = T^+ e^{ikL}, \qquad p(x)\big|_{x=L} = R^+ + 1, \tag{4.24}$$

$$v_x(x)\big|_{x=0} = -\frac{T^+ e^{ikL}}{Z_0}, \qquad v_x(x)\big|_{x=L} = \frac{R^+ - 1}{Z_L}, \tag{4.25}$$

for an incident plane wave coming from $+\infty$ and propagating in the $-x$ direction, where $Z_0 = \rho_0 c_0$ and $Z_L = \rho_L c_L$ are the impedances of the media on either side of the structure, i.e., $x < 0$ and $x > L$, respectively.

Combining (4.22)–(4.25) with (4.20)–(4.21), we obtain the following relations:

$$T^- = \frac{1 + R^-}{T_{11} + T_{12}/Z_L}, \tag{4.26}$$

$$T^- = \frac{1 - R^-}{T_{21} Z_0 + T_{22} Z_0 / Z_L}, \tag{4.27}$$

$$T^+ = T_{11}\left(1 + R^+\right) + \frac{T_{12}}{Z_L}\left(R^+ - 1\right), \tag{4.28}$$

$$T^+ = -T_{21} Z_0 \left(1 + R^+\right) - T_{22} \frac{Z_0}{Z_L}\left(R^+ - 1\right). \tag{4.29}$$

In the following, we will obtain the relation between the elements of the **S**-matrix and those of the **T**-matrix in specific configurations:

(i) *Non-reciprocal systems*
Structures in which the condition $T^- \neq T^+$ is fulfilled.

(ii) *Reciprocal systems*
Structures in which the condition $T^- = T^+$ is fulfilled.

(iii) *Reciprocal and symmetric systems*
Structures in which the conditions $T^+ = T^-$ and $R^- = R^+$ are fulfilled.

4.2.4.2 Non-reciprocal Systems

In a general case, we can combine (4.26)–(4.29) and get

$$T^- = \frac{2e^{ikL}}{T_{11} + T_{12}/Z_L + T_{21}Z_0 + T_{22}Z_0/Z_L}, \tag{4.30}$$

$$R^- = \frac{T_{11} + T_{12}/Z_L - T_{21}Z_0 - T_{22}Z_0/Z_L}{T_{11} + T_{12}/Z_L + T_{21}Z_0 + T_{22}Z_0/Z_L}, \tag{4.31}$$

$$T^+ = \frac{Z_0}{Z_L}\frac{2e^{ikL}\left(T_{11}T_{22} - T_{12}T_{21}\right)}{T_{11} + T_{12}/Z_L + T_{21}Z_0 + T_{22}Z_0/Z_L}, \tag{4.32}$$

$$R^+ = \frac{-T_{11} + T_{12}/Z_L - T_{21}Z_0 + T_{22}Z_0/Z_L}{T_{11} + T_{12}/Z_L + T_{21}Z_0 + T_{22}Z_0/Z_L}. \tag{4.33}$$

Equations (4.30)–(4.33) give the relation between the **T**-matrix and the **S**-matrix in the general form. However, some simplifications can be done.

4.2.4.3 Reciprocal Systems

The reciprocal behaviour of the system implies that the determinant of transfer matrix is the unity, i.e., $T_{11}T_{22} - T_{12}T_{21} = 1$. This property is satisfied by linear and time-invariant systems where the transmission does not depend on the direction of incident wave. These conditions are satisfied by most of the acoustic materials. Note this term appears in (4.32) and directly implies the transmission coefficients are identical whatever the direction of excitation. Therefore, in reciprocal systems

$$T^- = T^+ = T. \tag{4.34}$$

All the systems considered in this chapter are reciprocal. Note that in this case, the **S**-matrix, (4.19), possesses two eigenvalues given by

$$\lambda_{1,2} = T \pm \sqrt{R^+R^-}, \tag{4.35}$$

while the eigenvectors corresponding to λ_1 and λ_2 are

$$\vec{v}_1 = \left[\sqrt{R^+R^-}, R^+\right], \quad \vec{v}_2 = \left[R^-, -\sqrt{R^+R^-}\right], \tag{4.36}$$

respectively. The poles and zeros of the eigenvalues as well as the eigenvectors of the **S**-matrix in the complex-frequency plane provide rich information, as they are

identified with the resonances of the system. A further description of the eigenvalues of the scattering matrix and its implications for perfect absorption are given in Chap. 5.

In addition, in most cases in acoustics the structure is surrounded by the same media $Z_0 = Z_L$, as occurs in metamaterials surrounded by air. Under this additional condition, the reflection and transmission coefficients given by (4.30)–(4.33) can be simplified to

$$T = \frac{2e^{ikL}}{T_{11} + T_{12}/Z_0 + T_{21}Z_0 + T_{22}}, \tag{4.37}$$

$$R^- = \frac{T_{11} + T_{12}/Z_0 - T_{21}Z_0 - T_{22}}{T_{11} + T_{12}/Z_0 + T_{21}Z_0 + T_{22}}, \tag{4.38}$$

$$R^+ = \frac{-T_{11} + T_{12}/Z_0 - T_{21}Z_0 + T_{22}}{T_{11} + T_{12}/Z_0 + T_{21}Z_0 + T_{22}}. \tag{4.39}$$

When the materials that constitute the acoustic structure present intrinsic losses, e.g., thermoviscous or viscoelastic ones, a portion of the energy is neither reflected nor transmitted: it is absorbed by the structure and irreversibly transformed into heat. The amount of absorbed energy, dissipated by intrinsic losses, with respect to the total energy is characterized by the absorption coefficient, $\alpha(\omega)$. For asymmetric systems $R^+ \neq R^-$ and, therefore, the absorption depends on the direction of propagation. For the positive x-axis incident wave, the absorption is given by

$$\alpha^- = 1 - \left|R^-\right|^2 - |T|^2, \tag{4.40}$$

while for the negative x-axis incident waves,

$$\alpha^+ = 1 - \left|R^+\right|^2 - |T|^2. \tag{4.41}$$

4.2.4.4 Symmetric Systems

For symmetric systems such as structures presenting a mirror symmetry with respect to $x = L/2$, the transfer matrix coefficients fulfil

$$T_{11} = T_{22}. \tag{4.42}$$

As a consequence, the reflection coefficients from both sides are the same, i.e., $R^+ = R^- = R$. The absorption coefficients from both sides of the system are thus identical and correspond to

$$\alpha^+ = \alpha^- = \alpha = 1 - |R|^2 - |T|^2. \tag{4.43}$$

4.2.4.5 Reflection Problems

When the system is rigidly backed, a rigid boundary condition $v_x|_{x=L} = 0$ is applied in (4.11) and, obviously, no waves are transmitted through the system, i.e. $T = 0$ in (4.19). Therefore, we obtain the following relations

$$p(x)\big|_{x=0} = T_{11}\, p(x)\big|_{x=L}, \tag{4.44}$$

$$v_x(x)\big|_{x=0} = T_{21}\, p(x)\big|_{x=L}. \tag{4.45}$$

The reflection coefficient is related to the pressure and velocity at $x = 0$ as

$$p(x)\big|_{x=0} = 1 + R^-, \tag{4.46}$$

$$v_x(x)\big|_{x=0} = \frac{1 - R^-}{Z_0}. \tag{4.47}$$

Combining (4.44)–(4.45) with (4.46)–(4.47), the reflection coefficient for a rigidly-backed system becomes:

$$R = \frac{T_{11} - T_{21} Z_0}{T_{11} + T_{21} Z_0}. \tag{4.48}$$

The absorption coefficient of the rigidly-backed system is

$$\alpha = 1 - |R|^2 . \tag{4.49}$$

Finally, note that, if a rigid boundary condition is set at the beginning of the structure, $x = 0$, as $v_x|_{x=0} = 0$, and a wave impinges the structure from the opposite direction, i.e., a wave travelling in the $-x$ direction, the reflection coefficient is given by $R = (T_{22} - T_{21} Z_L)/(T_{22} + T_{21} Z_L)$.

4.2.4.6 Specific Acoustic Impedance

Note that the *characteristic* acoustic impedance, $Z_{\text{eff}} = \rho_{\text{eff}} c_{\text{eff}}$, is generally different from the *specific* acoustic impedance, $Z = p/v_x$. The characteristic impedance is a property of the material itself and does not depend on the boundary conditions at $x = 0$ and $x = L$. In the opposite, the effects of the boundary conditions are implicit for the acoustic impedance.[1] One important magnitude is the *specific* acoustic impedance of the system at the input of the system, or normal acoustic specific impedance, given by,

[1] Note that $Z = Z_{\text{eff}}$, i.e., $p/v_x = \rho_{\text{eff}} c_{\text{eff}}$, only stands for plane waves travelling in an infinite medium.

$$Z_{\text{in}} = \left.\frac{p}{v_x}\right|_{x=0}. \tag{4.50}$$

For transmission problems, it can be calculated directly from the reflection and transmission coefficients as

$$Z_{\text{in}} = Z_0 \left(\frac{1+R}{1-R}\right)\left(\frac{1+T}{1-T}\right). \tag{4.51}$$

For rigidly-backed problems this expression reduces to

$$Z_{\text{in}} = Z_0 \left(\frac{1+R}{1-R}\right). \tag{4.52}$$

This quantity is very useful to analyse the impedance matching of a given structure with the surrounding media.

4.3 Review of the Usual Transfer Matrices

A given system can be subdivided in N elements of respective transfer matrices $\mathbf{T}_n$, $n = 1, ..., N$ to evaluate its full transfer matrix $\mathbf{T}$. Depending on the nature of each element, its individual transfer matrix is calculated in different way. In the following, we review the most usual transfer matrices used to solve 1D problems in acoustics.

4.3.1 Particle Velocity Verses Flow Formulation

First of all, we shall differentiate the problem of wave propagation through layers of fluids or fluid-like materials of undefined section, with the problem of wave propagation through fluids confined in ducts of finite cross-sectional area, as shown in Fig. 4.4.

4.3.1.1 Particle Velocity Formulation

For layers of undefined section, Fig. 4.4a, the problem can be described by using the *particle-velocity formulation*, as given in the previous section. For example, this is the case when considering multilayer porous material absorbers.

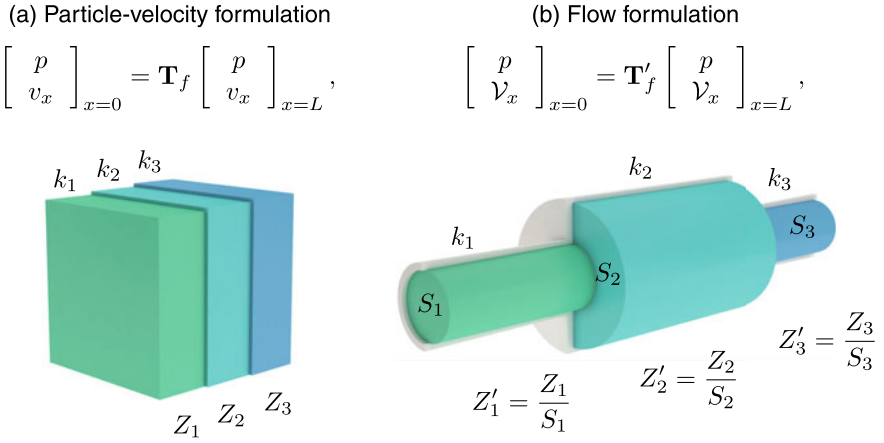

Fig. 4.4 **a** Formulation of the problem for layers of fluid-like materials of undefined section, i.e., particle-velocity formulation. **b** Formulation of the problem for waveguides of different cross-sectional areas, i.e., flow formulation

4.3.1.2 Flow Formulation

However, when considering waveguides of different cross-section, Fig. 4.4b, as it is usual when describing mufflers, metamaterials or similar structures, it is convenient to formulate the problem using the *flow*.

4.3.2 Fluid Layers: Particle Velocity Formulation

The transmission matrix $\mathbf{T}_f$ of a fluid layer of length L takes the form

$$\mathbf{T}_f = \begin{bmatrix} \cos(k_f L) & i Z_f \sin(k_f L) \\ i \dfrac{1}{Z_f} \sin(k_f L) & \cos(k_f L) \end{bmatrix}, \tag{4.53}$$

where $k_f = \omega/\sqrt{K_f/\rho_f}$ and $Z_f = \sqrt{K_f \rho_f}$ are wavenumber and the characteristic impedance in the fluid, respectively, where K_f and ρ_f are the effective bulk modulus and mass density of the fluid. Note that, in general, when losses are accounted for, K_f and ρ_f, and thus k_f and Z_f are complex and frequency dependent variables.

The intrinsic losses can be neglected in the case of sound confined in a cavity, e.g., an air cavity between two walls, if the size of the latter is much larger than the thicknesses of the viscous and thermal boundary layers of the fluid. The wavenumber in the fluid thus reduces to $k_f = \omega/c_0$, and the acoustic impedance becomes $Z_f =$

$\rho_0 c_0$, where the sound speed is $c_0 = \sqrt{K_0/\rho_0}$, with ρ_0 and K_0 respectively the density and bulk modulus of the lossless fluid.

However, the intrinsic losses of the fluid should be accounted for in highly viscous fluids, when sound wave is propagating over a long path, i.e., when the attenuation along the propagation path L is not negligible, and at high frequencies.

4.3.2.1 Thermoviscous Fluid Layers

Before considering confined sound propagation, note that, even in the absence of boundaries, the propagation of acoustic waves in fluid with a high viscosity is characterized by a complex wavenumber and impedance, which take the form [31]

$$k_f(\omega) = \frac{\omega}{c_0} + i\frac{b\omega^2}{2\rho_0 c_0^3}, \quad Z_f(\omega) = \rho_0 \frac{\omega}{k_f}, \tag{4.54}$$

where $b = \eta + (4/3)\mu + \kappa\left(C_V^{-1} - C_P^{-1}\right)$ is the diffusion coefficient, η and μ are the shear and bulk viscosities, κ the thermal conductivity of the thermoviscous fluid and C_V and C_P are the heat capacity at constant volume and pressure, respectively. Note the losses in the thermoviscous fluid show a quadratic dependence on frequency. Thus, the imaginary part of the complex wavenumber can be neglected for relatively low frequencies.

4.3.3 Ducts: Flow Formulation

When the fluid is confined in ducts or cavities, i.e., waveguides of different cross-sectional area, reflections are produced at the discontinuities. In this case, it is convenient to formulate the transfer matrix considering the flux,

$$\mathcal{V}_x = S v_x, \tag{4.55}$$

across a cross-sectional area S instead of using the particle velocity, v_x. The transfer matrix for the flow formulation, $\mathbf{T}'_f$, relates the pressure and flow at the inlet and at the outlet of the waveguide of length L as

$$\begin{bmatrix} p \\ \mathcal{V}_x \end{bmatrix}_{x=0} = \mathbf{T}'_f \begin{bmatrix} p \\ \mathcal{V}_x \end{bmatrix}_{x=L}. \tag{4.56}$$

By substituting (4.55) in (4.7)–(4.8) we can obtain the transfer matrix of a waveguide or duct for the flow formulation as

$$\mathbf{T}'_f = \begin{bmatrix} \cos(k_f L) & i Z'_f \sin(k_f L) \\ i \dfrac{1}{Z'_f} \sin(k_f L) & \cos(k_f L) \end{bmatrix}, \tag{4.57}$$

where $Z'_f = Z_f / S$ is the normalized impedance. Note this matrix is equivalent to the one given by (4.53): the impedances appearing in the transfer matrix are divided by S, while the wavenumbers are not modified. In addition, transfer matrices of varying cross-section waveguides, e.g., conical, are also available in the literature [32–34].

On the one hand, to calculate the effective wavenumber for the flow problem (4.15) holds. However, to calculate the effective impedance for a flow formulation, instead of (4.16), the following equation must be used

$$Z_{\text{eff}} = S \sqrt{\frac{T_{12}}{T_{21}}}. \tag{4.58}$$

On the other hand, the transmission and reflection coefficients for the flow formulation can be obtained in a straightforward manner: one might use normalized impedances instead of impedances. For example, the scattering for the flow formulation corresponding to the non-reciprocal case can be obtained by changing Z by Z/S in (4.30)–(4.33).

In addition, if the fluid is confined in a narrow duct or cavity, strong losses are observed when the transversal dimension of the cavity is of the same order of the thermal and/or viscous boundary layers. The thermal and viscous layers are given by

$$\delta_{\text{thermal}} = \sqrt{\frac{2\kappa}{\omega C_P}}, \quad \delta_{\text{viscous}} = \sqrt{\frac{2\eta}{\omega \rho_0}}, \tag{4.59}$$

therefore, $\delta_{\text{viscous}} = \sqrt{\text{Pr}}\, \delta_{\text{thermal}}$, where $\text{Pr} = C_P \eta / \kappa$ is the Prandtl number. One approach to include the thermoviscous loses in the TMM is to model the fluid inside the duct as an equivalent fluid with effective parameters, therefore $\rho_f(\omega)$, $K_f(\omega) \in \mathbb{C}$, and they depend on the geometry and dimensions of the duct.

4.3.3.1 Slits

When considering the propagation of acoustic waves in narrow slits, as shown in Fig. 4.5, the thermoviscous losses should be accounted for if the length of the thermal and/or viscous boundary layers are of the same order of the slit height. Instead of solving the full Navier-Stokes equations with non-slip boundary conditions, the thermoviscous losses can be modelled by using effective complex and frequency dependent parameters accounting for both attenuation and dispersion.

Thus, assuming that only plane waves propagate inside a slit, the complex effective parameters expressed as [35]:

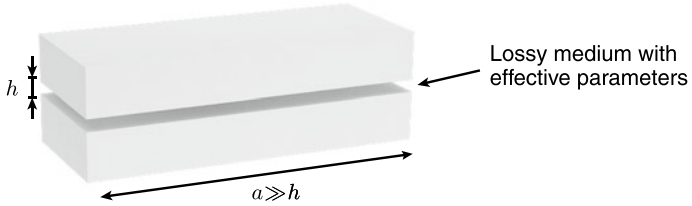

Fig. 4.5 Slit of height h. The system is modelled as a fluid-like medium with effective properties: complex and frequency dependent effective parameters

$$\rho_f(\omega) = \rho_0 \left[1 - \frac{\tanh \frac{h}{2} G_\rho(\omega)}{\frac{h}{2} G_\rho(\omega)} \right]^{-1}, \tag{4.60}$$

$$K_f(\omega) = K_0 \left[1 + (\gamma - 1) \frac{\tanh \frac{h}{2} G_K(\omega)}{\frac{h}{2} G_K(\omega)} \right]^{-1}, \tag{4.61}$$

where h is the width of the slit.

The functions $G_\rho(\omega)$ and $G_K(\omega)$ are

$$G_\rho(\omega) = \sqrt{\frac{i\omega\rho_0}{\eta}}, \tag{4.62}$$

$$G_K(\omega) = \sqrt{\frac{i\omega \mathrm{Pr}\rho_0}{\eta}}, \tag{4.63}$$

and $\gamma = C_P/C_V$ is the ratio of specific heats of the fluid, $K_0 = \gamma P_0$ is the adiabatic bulk modulus with P_0 the static pressure, η the dynamic viscosity and ρ_0 the density. The normalized acoustic impedance, for a 2D problem, is given by $Z'_f = \sqrt{K_f \rho_f}/ah$, where a is the width of the slit that must fulfil $a \gg h$, as shown in Fig. 4.5. In the case of slits of small a, its effective parameters must be calculated as a rectangular waveguide (see Sect. 4.3.3.3 below).

4.3.3.2 Cylindrical Cross-Section Ducts

In the same way, the propagation of acoustic waves in a narrow cylindrical duct, as shown in Fig. 4.6, can be described via a complex and frequency dependent density and bulk modulus given by [35].

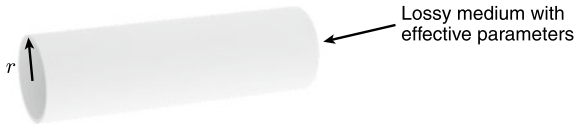

Fig. 4.6 Cylindrical cross-sectional duct of radius r

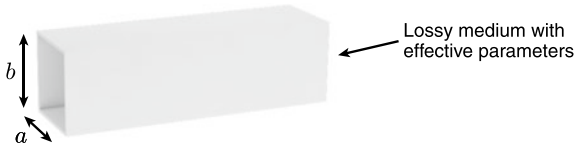

Fig. 4.7 Rectangular cross-section duct of sides a and b

$$\rho_f(\omega) = \rho_0 \left[1 - \frac{2}{rG_\rho(\omega)} \frac{J_1(rG_\rho(\omega))}{J_0(rG_\rho(\omega))} \right]^{-1}, \tag{4.64}$$

$$K_f(\omega) = K_0 \left[1 + \frac{2(\gamma - 1)}{rG_K(\omega)} \frac{J_1(rG_K(\omega))}{J_0(rG_K(\omega))} \right]^{-1}, \tag{4.65}$$

where r is the radius of the cylindrical duct, J_n is the Bessel function of the first kind and order n, and the functions $G_\rho(\omega)$ and $G_K(\omega)$ are given by (4.62)–(4.63). In this case, the normalized acoustic impedance is given by $Z'_f = \sqrt{K_f \rho_f}/\pi r^2$.

It is important to note that TMM calculations should be restricted for frequencies lower that the cut-off frequency of the cylindrical duct, i.e., in the range given by $\omega < 1.84 c_0/r$. For higher frequencies the duct can exhibit high-order modes and the plane-wave approximation does not hold.

4.3.3.3 Rectangular Cross-Section Ducts

Finally, again assuming that only plane waves propagate inside a rectangular cross-sectional duct, as depicted Fig. 4.7, the propagation can be modelled with effective density and bulk modulus given by [35].

$$\rho_f(\omega) = \rho_0 \frac{(a/2)^2 (b/2)^2}{4G_\rho^2(\omega) \sum_{m\in\mathbb{N}} \sum_{n\in\mathbb{N}} \left[\alpha_m^2 \beta_n^2 \left(\alpha_m^2 + \beta_n^2 - G_\rho^2(\omega) \right) \right]^{-1}}, \tag{4.66}$$

$$K_f(\omega) = K_0 \frac{1}{\gamma + \frac{4(\gamma-1)G_K^2(\omega)}{(a/2)^2(b/2)^2} \sum_{m\in\mathbb{N}} \sum_{n\in\mathbb{N}} \left[\alpha_m^2 \beta_n^2 \left(\alpha_m^2 + \beta_n^2 - G_K^2(\omega) \right) \right]^{-1}}, \tag{4.67}$$

where a and b are the dimensions of the rectangular duct, $\alpha_m = (2m+1)\pi/a$ and $\beta_n = (2n+1)\pi/b$. The acoustic impedance is $Z'_f = \sqrt{K_f \rho_f}/ab$.

The frequency range where the plane-wave assumption is valid for a rectangular duct is given by $\omega < \pi c_0 / \max(a, b)$. As occur in the cylindrical duct, at higher

frequencies the waveguide can exhibit high-order modes and TMM calculations will be inaccurate.

4.3.4 Porous Media Layers

Porous materials are biphasic materials composed of a solid frame filled with a fluid, generally air. Typically, the pore size of foams or fibrous materials is much smaller than the characteristic wavelength of the sound waves. Thus, the complex processes occurring during the propagation of acoustic waves at the micro-scale can be modelled at the macro-scale via an effective medium with effective properties. Although elastic waves can propagate in the solid frame, the solid skeleton can be considered motionless in most practical cases in acoustics because of its high impedance contrast with the light saturating fluid, e.g. the air. In this way, the waves emerging from the interaction of elastic waves in the solid matrix and acoustic waves in the saturating fluid, i.e., the Biot waves, can be neglected. Under this assumption, a layer of porous material can be modelled as an equivalent fluid with effective density and bulk modulus. This is generally accurate for thick porous layers because flexural modes appear at very high frequencies and are then strongly attenuated.

The transfer matrix of a porous layer, $\mathbf{T}_p$, is thus written as

$$\mathbf{T}_p = \begin{bmatrix} \cos(k_p L_p) & i Z_p \sin(k_p L_p) \\ i \dfrac{1}{Z_p} \sin(k_p L_p) & \cos(k_p L_p) \end{bmatrix}, \tag{4.68}$$

where Z_p and k_p are the characteristic effective impedance and wavenumber of the porous material. These effective properties are complex and frequency dependent and several models have been developed providing comprehensive expressions. These models usually consider parameters of the structural properties of the porous frame, in addition to the thermoviscous properties of the saturating fluid (Fig. 4.8).

Accurate models with many input parameters are required to account for most of the physics concerning the thermoviscous processes. However, simpler models relying on a reduced number of input parameters are available, also providing a lower accuracy and possessing a thinner frequency range of validity. Models with a reduced number of parameters are generally sufficient (and practical in most cases), because the input parameters are usually difficult to estimate and the samples are not exactly identical due to the random nature of the porous structure. In the following, we will review several models relying on one, five and six input parameters.

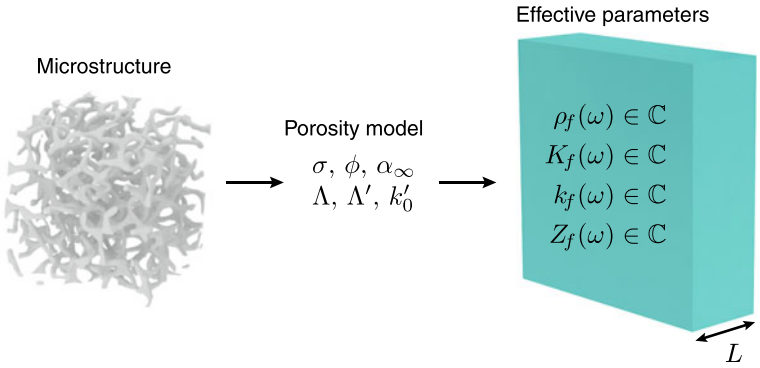

Fig. 4.8 The complex structure of a porous material in the micro-scale can be described by several input parameters. Then, complex and frequency dependent expressions for the effective parameters can be obtained

4.3.4.1 Empirical Models

One of the simplest models of porous materials is the one-parameter model proposed by Delany-Bazley (D&B) [36]. This unique parameter is the flow resistivity σ. This model was derived by fitting the measured characteristic impedance and wavenumber of a wide variety of porous materials with porosity close to the unit and flow resistivity covering the range $1 < \sigma < 50$ kNs/m^4 with a power law of $\rho_0 f/\sigma$. The model validity is thus $0.01 < \rho_0 f/\sigma < 1$.

The complex and frequency dependent effective wavenumber and characteristic impedance are given by

$$Z_p(\omega) = Z_0 \left[1 + a_1^z \left(\frac{\rho_0 \omega}{2\pi\sigma} \right)^{b_1^z} - i a_2^z \left(\frac{\rho_0 \omega}{2\pi\sigma} \right)^{b_2^z} \right], \tag{4.69}$$

$$k_p(\omega) = k_0 \left[1 + a_1^k \left(\frac{\rho_0 \omega}{2\pi\sigma} \right)^{b_1^k} - i a_2^k \left(\frac{\rho_0 \omega}{2\pi\sigma} \right)^{b_2^k} \right], \tag{4.70}$$

where the coefficients a_1^z, a_2^z, b_1^z, b_2^z, a_1^k, a_2^k, b_1^k, b_2^k are given in Table 4.1. It is worth noticing here that the behaviour of some porous materials does not exactly follow this model.

This approach has been extended by several authors. Table 4.1 summarizes alternative empirical models where the coefficients were fitted for specific types of porous and fibrous materials: Dunn and Davern [38] obtained the coefficients for polyurethane foams of low flow resistivity, Qunli [39] for porous plastic open-cell foams, Kirby and Cummings[42] for fibrous materials A glass, E glass, basalt wool and steel wool, Muehleisen et al. [41] for highly porous, rigid and open cell carbon foams, (reticulated vitreous carbon), and finally Garai and Pompoli [43] for polyester fibrous materials.

Table 4.1 Coefficients of empirical models to calculate the effective parameters of porous materials using [*Use (4.71)–(4.72)]. Courtesy of Rodolfo Venegas

Model		a_1^z	a_2^z	b_1^z	b_2^z	a_1^k	a_2^k	b_1^k	b_2^k
D&B [36]		0.0571	−0.087	−0.754	−0.732	0.0978	−0.189	−0.7	−0.595
Mechel [37]	$X < 0.025$	0.0688	−0.196	−0.707	−0.549	0.135	−0.396	−0.646	−0.458
	$X \geq 0.025$	0.0235	−0.0875	−0.887	−0.77	0.102	−0.179	−0.705	−0.674
Dunn&Davern [38]		0.114	−0.099	−0.369	−0.758	0.136	−0.168	−0.491	−0.715
Qunli [39]		0.212	−0.105	−0.607	−0.607	0.163	−0.188	−0.592	−0.544
Miki* [40]		0.07	−0.107	−0.632	−0.632	0.109	−0.16	−0.618	−0.618
Muehleisen et al. [41]		0.2283	−0.1803	−0.4884	−0.8155	0.0898	−0.2049	−0.8453	−−0.7215
K&C A glass [42]		0.0924	−0.1457	−0.7177	−0.5951	0.1443	−0.2251	−0.7088	−0.5827
K&C E glass [42]		0.0954	−0.1689	−0.6687	−0.5707	0.2010	−0.2202	−0.5829	−0.5850
K&C Basalt wool [42]		0.0599	−0.1376	−0.7664	− 0.6276	0.1281	−0.2178	−0.6746	−0.6051
K&C Steel wool [42]		0.0877	−0.0876	−0.5557	− 0.7609	0.1328	−0.1540	−0.5571	−0.7093
G&P [43]		0.078	−0.074	−0.623	−0.660	0.121	−0.159	−0.530	−0.571

In particular, a further refinement of the D&B model was carried out by Miki [40], using same data as those used to derive the D&B model, to correct non-physical behaviour of the effective properties in the low frequency regime. The equations for this model are

$$Z_p(\omega) = Z_0\left[1 + a_1^z\left(\frac{\omega}{2\pi\sigma}\right)^{b_1^z} - ia_2^z\left(\frac{\omega}{2\pi\sigma}\right)^{b_2^z}\right], \tag{4.71}$$

$$k_p(\omega) = k_0\left[1 + a_1^k\left(\frac{\omega}{2\pi\sigma}\right)^{b_1^k} - ia_2^k\left(\frac{\omega}{2\pi\sigma}\right)^{b_2^k}\right], \tag{4.72}$$

and the range of validity is then enlarged to $0.01 < f/\sigma < 1$. The model proposed by Miki should be used instead of the original proposed by Delany and Bazley.

4.3.4.2 Semi-empirical Models

Another widely used class of equivalent models for porous materials is the semi-empirical one. These models attempt to link high and low frequency asymptotic exact behaviours of porous material by simple functions and rely on the separation of viscous (in the density) and thermal (in the bulk modulus) losses. Among several, the Johnson-Champoux-Allard and the Johnson-Champoux-Allard-Lafarge models are the most commonly encountered.

4.3.4.3 The Johnson-Champoux-Allard Model

The Johnson-Champoux-Allard (JCA) model [44, 45] involves 5-parameters and provides the expressions of the dynamic effective density and bulk modulus of a porous material saturated by a fluid of density ρ_0 and bulk modulus K_0 considering a rigid frame. The porous material is characterized by its porosity, ϕ, its tortuosity, α_∞, its flow resistivity, σ, and the thermal and viscous characteristic lengths, Λ' and Λ respectively.

The dynamic effective density and bulk modulus given by the JCA model are

$$\rho_p(\omega) = \rho_0\frac{\alpha_\infty}{\phi}\left[1 - iG_1(\omega)\sqrt{1 + iG_2(\omega)}\right], \tag{4.73}$$

$$K_p(\omega) = K_0\frac{\phi^{-1}}{\gamma - (\gamma-1)\left[1 - iG_1'(\omega)\sqrt{1 + iG_2'(\omega)}\right]^{-1}}, \tag{4.74}$$

where the adiabatic bulk modulus is given by $K_0 = \gamma P_0$. A description of the physical meaning and the measurement procedure for the input parameters can be found in the literature [2, 46].

The functions $G_1(\omega)$, $G_2(\omega)$, $G_1'(\omega)$, $G_2'(\omega)$ are given by

$$G_1(\omega) = \frac{\sigma\phi}{\alpha_\infty \rho_0 \omega}, \tag{4.75}$$

$$G_2(\omega) = \frac{4\alpha_\infty^2 \rho_0 \eta \omega}{\sigma^2 \phi^2 \Lambda^2}, \tag{4.76}$$

$$G_1'(\omega) = \frac{8\eta}{\rho_0 \mathrm{Pr} \Lambda'^2 \omega}, \tag{4.77}$$

$$G_2'(\omega) = \frac{\rho_0 \mathrm{Pr} \Lambda'^2 \omega}{16\eta}. \tag{4.78}$$

Using these expressions, both the effective wavenumber and the characteristic acoustic impedance of the porous material can be obtained by using

$$k_p = \frac{\omega}{c_p} = \omega \sqrt{\frac{\rho_p}{K_p}}, \tag{4.79}$$

where c_p is the effective sound speed in the porous material and

$$Z_p = \sqrt{\rho_p K_p}. \tag{4.80}$$

4.3.4.4 The Johnson-Champoux-Allard-Lafarge Model

The JCA model was further be extended by Lafarge [47] to accurately describe the thermal effects in the low frequency regime. The extended model, namely the Johnson-Champoux-Allard-Lafarge (JCAL) model, involves a new parameter, the static thermal permeability, k_0'. Only the bulk modulus is modified when compared to the JCA model and $G_1'(\omega)$ and $G_2'(\omega)$ read as

$$G_1'(\omega) = \frac{\phi\eta}{\rho_0 \mathrm{Pr} k_0' \omega}, \tag{4.81}$$

$$G_2'(\omega) = \frac{4\mathrm{Pr}\rho_0 k_0'^2 \omega}{\eta \phi^2 \Lambda'^2}. \tag{4.82}$$

Please note that the JCAL model is usually written in terms of the static viscous permeability $k_0 = \eta/\sigma$ which is an intrinsic parameter of the material. In this case $G_1(\omega)$ and $G_2(\omega)$ become

$$G_1(\omega) = \frac{\phi\eta}{\alpha_\infty \rho_0 k_0 \omega}, \tag{4.83}$$

$$G_2(\omega) = \frac{4\alpha_\infty^2 \rho_0 k_0^2 \omega}{\eta\phi^2 \Lambda^2}. \tag{4.84}$$

4.3.5 Locally Resonant Elements

The previously described elements only considered continuity of pressure and flux along the main propagation direction. However, some elements can be added to the transmission line that rely on pressure drop or flux continuity in other directions and are usually locally resonant elements.

Let us assume an element of lateral dimension Δx much smaller than the wavelength along the main waveguide. This element can be considered as a punctual resonator. The upstream and downstream pressure, p_u and p_d, and flux, $\mathcal{V}_d$ and $\mathcal{V}_u$, are first introduced allowing to define the transfer matrix of this infinitesimal element.

$$\begin{bmatrix} p_d \\ \mathcal{V}_d \end{bmatrix}_x = \mathbf{T}' \begin{bmatrix} p_u \\ \mathcal{V}_u \end{bmatrix}_{x+\Delta x}, \tag{4.85}$$

The pressure drop

$$\Delta p = p_d - p_u, \tag{4.86}$$

and flux continuity

$$\Delta \mathcal{V} = \mathcal{V}_d - \mathcal{V}_u, \tag{4.87}$$

can subsequently be defined as a function of the resonator.

4.3.5.1 Side-Branch (Parallel) Elements

On the one hand, locally resonant elements can load the main waveguide, as shown in Fig. 4.9. This loading element can be an open or closed duct, a Helmholtz resonator, or a dead-end cavity of any complex shape. In this case, the pressure is constant along the element, i.e., $\Delta p = 0$ or $p_d = p_u$, while the flux continuity implies $\Delta \mathcal{V} = \mathcal{V}_d - \mathcal{V}_u = p_u / Z_r'$, where Z_r' is the resonator impedance. Please note that the continuity of pressure has already been accounted for in the last expression.

The equations relating pressures and velocities at both sides of the infinitesimal element are then

$$p_d = p_u, \tag{4.88}$$

$$v_d = v_u + p_u / Z_r, \tag{4.89}$$

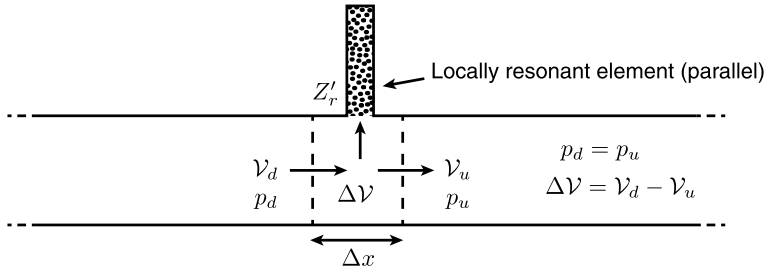

Fig. 4.9 Parallel configuration with a locally resonant element loaded in a waveguide. The resonator introduces a *flow drop* while pressure is continuous

which can be re-written in matrix form to give the transmission matrix for "parallel" connected elements, $\mathbf{T}'$, as

$$\mathbf{T}' = \begin{bmatrix} 1 & 0 \\ \dfrac{1}{Z'_r} & 1 \end{bmatrix}. \tag{4.90}$$

4.3.5.2 In-Line (Series) Elements

On the other hand, locally resonant elements can be in series in a main waveguide, as shown in Fig. 4.10. For example, this series elements can be membranes or elastic plates located in a waveguide.

This time the flux is continuous across the infinitesimal element, i.e., $\Delta\mathcal{V} = 0$ or $\mathcal{V}_d = \mathcal{V}_u$, but the punctual resonator induces a pressure drop $\Delta p = p_d - p_u = Z'_r \mathcal{V}_u$, where Z'_r is the resonator impedance. Please note that the flux continuity has already been applied. The equations relating pressures and velocities at both sides are

$$p_d = p_u + Z'_r v_u, \tag{4.91}$$
$$\mathcal{V}_d = \mathcal{V}_u, \tag{4.92}$$

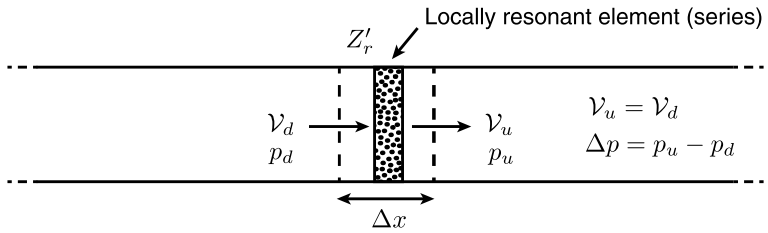

Fig. 4.10 Series configuration with a locally resonant element located in-line in a waveguide. The resonator introduces a *pressure drop* while flow is continuous

an can then be written in matrix form to obtain the transfer matrix of "series" elements $\mathbf{T}'$ as

$$\mathbf{T}' = \begin{bmatrix} 1 & Z'_r \\ 0 & 1 \end{bmatrix}. \tag{4.93}$$

In the following subsections we will review particular impedance expressions of different resonators that are commonly arranged in-series or in-parallel to waveguides.

4.3.6 Side Resonating Ducts

When a waveguide is loaded by a secondary duct of length l, as shown for example in Fig. 4.11 for a sealed secondary duct, the pressure and flux at $z = 0$ and $z = l$ can be related by a transfer matrix of the form

$$\begin{bmatrix} p \\ \mathcal{V}_z \end{bmatrix}_{z=0} = \begin{bmatrix} \cos(k_f l) & i Z'_f \sin(k_f l) \\ i \dfrac{1}{Z'_f} \sin(k_f l) & \cos(k_f l) \end{bmatrix} \begin{bmatrix} p \\ \mathcal{V}_z \end{bmatrix}_{z=l}. \tag{4.94}$$

where $Z'_f = Z_f / S_f$ and k_f are the characteristic impedance and wavenumber, and S_f the cross-section area of the secondary duct. Note that thermoviscous losses in this duct can be accounted for using an appropriate complex and frequency dependent wavenumber and impedance, that can be calculated accordingly to (4.60)–(4.67) as a function of the cross-sectional geometry. Depending on the boundary condition at $z = l$, the input resonator impedance at $z = 0$ can be evaluated via $Z'_r = p(0)/\mathcal{V}_z(0)$.

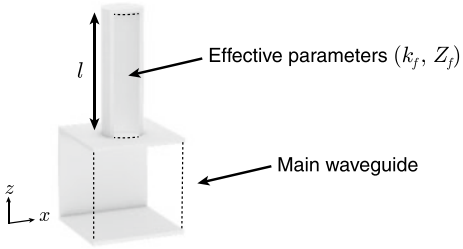

Fig. 4.11 Quarter-wavelength resonator (QWR), of length l, loaded on a main waveguide. Resonator is modelled using the complex and frequency dependent wavenumber and impedance that depend on the resonator geometry

4.3.6.1 Closed Secondary Duct: The Quarter-Wavelength Resonator (QWR)

When the secondary duct is sealed, i.e., a rigid boundary condition is applied at $z = l$, i.e., $\mathcal{V}_z(l) = 0$, the system of equations given by (4.94) reduces to

$$p(0) = \cos(k_f l)\, p(l) \quad \text{and} \quad \mathcal{V}_z(0) = i\frac{1}{Z_f}\sin(k_f l)\, p(l). \tag{4.95}$$

The input impedance is then

$$Z_r' = -i\, Z_f' \cot\left(k_f l\right) = -i\frac{Z_f}{S_f}\cot\left(k_f l\right), \tag{4.96}$$

where l is the QWR length. The first resonance is observed when $Z_r' = 0$, implying $\cot(k_f l) = 0$, i.e., $l \approx \lambda/4$ where λ is the wavelength (note k_f can be complex).

4.3.6.2 "End" Correction

Note that the well-known "end" correction must be incorporated to this impedance to account for the radiation of the resonator in the main waveguide. This radiation is modelled by adding a subwavelength, i.e. $k_0 \Delta l \ll 1$, fluid transfer matrix of length Δl, i.e., the end correction, with wavenumber and impedance k_0 and $Z_0' = Z_0/S$ of the main waveguide of section S to (4.94):

$$\begin{bmatrix} p \\ \mathcal{V}_z \end{bmatrix}_0 = \begin{bmatrix} \cos(k_0\Delta l) & i\, Z_0' \sin(k_0\Delta l) \\ i\dfrac{1}{Z_0'}\sin(k_0\Delta l) & \cos(k_0\Delta l) \end{bmatrix} \begin{bmatrix} \cos(k_f l) & i\, Z_f' \sin(k_f l) \\ i\dfrac{1}{Z_f'}\sin(k_f l) & \cos(k_f l) \end{bmatrix} \begin{bmatrix} p \\ \mathcal{V}_z \end{bmatrix}_l.$$

Taylor expanding the first matrix and applying the rigid boundary condition at $z = l$, (4.96) becomes

$$Z_r' = -i\frac{Z_f}{S_f}\cot\left(k_f l\right) - i\omega\rho_0\frac{\Delta l}{S}, \tag{4.97}$$

which is the input impedance of a QWR with "end" correction. The "end" corrections Δl are given in the Appendix 4.6.2.

4.3.6.3 Open Secondary Duct: The Half-Wavelength Resonator (HWR)

When the secondary duct is open, pressure-release boundary condition can be applied in (4.94) at $z = l$, i.e., $p(l) = 0$. This leads to the system of equations

$$p(0) = i Z_f \sin(k_f l)\, p(l), \tag{4.98}$$

$$\mathcal{V}_z(0) = \cos(k_f l)\, p(l). \tag{4.99}$$

The input impedance is then

$$Z_r' = i Z_f' \tan\left(k_f l\right) = i \frac{Z_f}{S_f} \tan\left(k_f l\right), \tag{4.100}$$

where l is the resonator length. The resonance is no longer achieved when the length of the duct is a quarter of the wavelength, but rather half of it, i.e. the system is a half-wavelength resonator (HWR). However, the present model for HWR is less accurate than the one for QWR because the radiation to the outer domain must be inaccurate, i.e., the system can no longer be one-dimensional.

4.3.7 Helmholtz Resonators

Another type of commonly used side-branch resonator is the Helmholtz one that comprises a neck coupled to a cavity, as sketched in Fig. 4.12. The input impedance of the Helmholtz resonator (HR) can also be derived by relating the pressure and flux at the beginning, $z = 0$, and at the end, $z = l = l_n + l_c$, of the system. The ducts corresponding to the neck and the cavity are characterized by their length l_n and l_c and their sections S_n and S_c, respectively. The transfer matrix problem is written as

$$\begin{bmatrix} p \\ \mathcal{V}_z \end{bmatrix}_0 = \begin{bmatrix} \cos(k_n l_n) & i Z_n' \sin(k_n l_n) \\ i \dfrac{1}{Z_n'} \sin(k_n l_n) & \cos(k_n l_n) \end{bmatrix} \begin{bmatrix} \cos(k_c l_c) & i Z_c' \sin(k_c l_c) \\ i \dfrac{1}{Z_c'} \sin(k_c l_c) & \cos(k_c l_c) \end{bmatrix} \begin{bmatrix} p \\ \mathcal{V}_z \end{bmatrix}_l.$$

Note that specific complex and frequency dependent effective parameters must be used for each element if thermoviscous losses are accounted for because the neck and the cavity are of different cross-sections: k_n and $Z_n' = Z_n / S_n$ for the neck, and k_c and

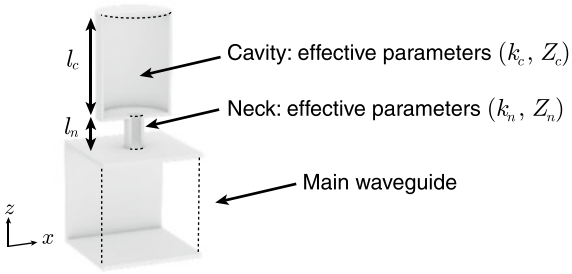

Fig. 4.12 Helmholtz resonator loaded on a main waveguide. The resonator is modelled using the complex and frequency dependent parameters that depend on its geometry

$Z'_c = Z_c/S_c$ for the cavity. Theses effective parameters are calculated accordingly to (4.60)–(4.67) as a function on the geometry of the ducts.

Applying rigid boundary condition at $z = l = l_n + l_c$, and manipulating the previous transfer matrix, the impedance of the HR can be written as $Z'_r = p(0)/\mathcal{V}_z(0)$

$$Z'_r = -iZ'_n \frac{Z'_c/Z'_n - \tan k_n l_n \tan k_c l_c}{Z'_c/Z'_n \tan k_n l_n + \tan k_c l_c}. \tag{4.101}$$

Taylor expanding the latter expression at low frequencies, i.e., $k_n l_n \ll 1$ and $k_c l_c \ll 1$, leads to

$$Z'_r = -iZ'_n \frac{Z'_c/Z'_n - k_n l_n k_c l_c}{Z'_c/Z'_n k_n l_n + k_c l_c}. \tag{4.102}$$

If losses are not considered, $k_n = k_c = k_0$ and $Z_n = Z_c = Z_0$, where $k_0 = \omega/c_0$ and $Z_0 = \rho_0 c_0$. The first resonance of the HR is then observed when $\mathrm{Im}(Z'_r) = 0$, leading to

$$\omega_R = c_0 \sqrt{\frac{S_n}{l_n l_c S_c}} = c_0 \sqrt{\frac{S_n}{l_n V_c}}, \tag{4.103}$$

which is the usual expression for the resonance frequency of a HR, where $V_c = S_c l_c$ is the volume of the cavity.

However, when thermoviscous losses are included such a compact expression cannot be derived. In this case the resonant frequency can be estimated numerically by looking for the frequency at which $\mathrm{Im}(Z'_r) = 0$ with the corresponding complex k_n, k_c, Z_n and Z_c. Usually, the so-calculated HR resonance frequency is moderately reduced as compared with (4.103).

It is worth noting here that (4.101) is not exact because corrections due to the radiation at the discontinuities must be included. Using a transfer matrix approach, see e.g., [48, Suppl. mat.], we can model the pressure radiation between the different elements. Thus, we can express the system as

$$\begin{bmatrix} p \\ \mathcal{V}_z \end{bmatrix}_0 = \begin{bmatrix} \cos(k_n \Delta l_2) & iZ'_n \sin(k_n \Delta l_2) \\ i\frac{1}{Z'_n} \sin(k_n \Delta l_2) & \cos(k_n \Delta l_2) \end{bmatrix} \begin{bmatrix} \cos(k_n l_n) & iZ'_n \sin(k_n l_n) \\ i\frac{1}{Z'_n} \sin(k_n l_n) & \cos(k_n l_n) \end{bmatrix} \times \ldots$$
$$\begin{bmatrix} \cos(k_n \Delta l_1) & iZ'_n \sin(k_n \Delta l_1) \\ i\frac{1}{Z'_n} \sin(k_n \Delta l_1) & \cos(k_n \Delta l_1) \end{bmatrix} \begin{bmatrix} \cos(k_c l_c) & iZ'_c \sin(k_c l_c) \\ i\frac{1}{Z'_c} \sin(k_c l_c) & \cos(k_c l_c) \end{bmatrix} \begin{bmatrix} p \\ \mathcal{V}_z \end{bmatrix}_l.$$

The first length correction, Δl_1, is due to pressure radiation at the discontinuity from the cavity to the neck of the HR [49], while the second length correction, Δl_2, comes from the radiation at the discontinuity from the neck to the principal waveguide [50]. Please note that rigorously, this second correction matrix should be written in terms

of the principal waveguide parameters, k_0 and Z_0'. However, replacing this parameters by those of the neck provides more accurate results. After application of the rigid boundary condition at $x = l$, Taylor expansion ($k_n \Delta l_1 \gg 1$ and $k_n \Delta l_2 \gg 1$) of the length correction matrices, and rearrangement, the impedance of the HR accounting for the "end" corrections becomes

$$Z_r' = -iZ_n' \frac{\cos k_n l_n \cos k_c l_c - \dfrac{k_n \Delta l Z_n'}{Z_c'} \cos k_n l_n \sin k_c l_c - \dfrac{Z_n'}{Z_c'} \sin k_n l_n \sin k_c l_c}{\sin k_n l_n \cos k_c l_c - \dfrac{k_n \Delta l Z_n'}{Z_c'} \sin k_n l_n \sin k_c l_c + \dfrac{Z_n'}{Z_c'} \cos k_n l_n \sin k_c l_c},$$

where the correction length $\Delta l = \Delta l_1 + \Delta l_2$ is the addition of the two correction lengths. The specific values for the correction lengths are given in the Appendix 4.6.1.

4.3.8 Rigid Micro-perforated Plates

When a rigid thin panel is densely perforated with holes whose dimensions are much smaller than the wavelength, it can be modelled as a local impedance that accounts for the wave propagation in the small ducts including the thermoviscous effects. Maa's model [51] consider a local impedance as

$$Z_r = -\frac{i\omega\rho_0 h}{\phi} \left[1 - \frac{2}{\sigma\sqrt{i}} \frac{J_1\left(\sigma\sqrt{i}\right)}{J_0\left(\sigma\sqrt{i}\right)} \right]^{-1} - i0.85\omega \frac{\rho_0 d}{\phi} + \frac{h\sqrt{2}\sigma\eta}{d\phi}, \tag{4.104}$$

where $\sigma = d\sqrt{\omega\rho_0/4\eta}$, d is the perforation diameter, h is the thickness of the plate, and $\phi = \pi d^2/4a^2$ is the surface porosity in case of circular perforation arranged in a square lattice of side a, as depicted in Fig. 4.13. The first term on right-hand-side of (4.104) accounts for the hole impedance, the second term models the reactive radiation at both appendicular parts of the perforation, while the purely resistive term models the friction at these appendicular parts. Note that the provided impedance is Z_r and not Z_r' and holds for a perforated plate of infinite lateral extends. An approximation of this model is given by

$$Z_r = -\frac{i\omega\rho_0 h}{\phi}\sigma_i + \frac{32\eta h}{\phi d^2}\sigma_\tau, \tag{4.105}$$

where the coefficients σ_i and σ_τ are given by

$$\sigma_i = 1 + \left[1 + \frac{\sigma^2}{2} \right]^{-\frac{1}{2}} + 0.85\frac{d}{h}, \quad \sigma_\tau = \sqrt{1 + \frac{\sigma^2}{32}} + \frac{4\sqrt{2}}{32}\sigma\frac{d}{h}. \tag{4.106}$$

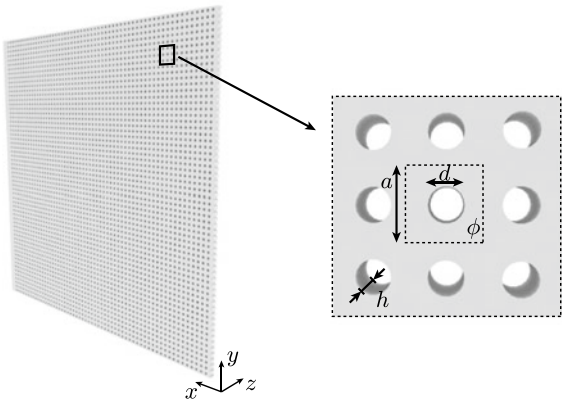

Fig. 4.13 Micro-perforated panel and the geometrical parameters used

This approximation is valid for $1 < \sigma < 10$. Further details, extended and alternative models can be found in [52].

4.3.9 Elastic Plates

Another type of often encountered locally resonant elements are elastic plates. The acoustic impedance of the plate relies on the pressure drop and flux continuity across the plate. Thus, different plate geometries and boundary conditions leads to different expressions for the acoustic impedance.

4.3.9.1 Circular Elastic Plate

Let us first consider a clamped circular plate of radius r and section $S = \pi r^2$, as the one depicted Fig. 4.14a. Note the clamped condition implies that the transverse displacement and its first normal derivative vanish at the plate boundary. Assuming that only the axisymmetric modes can be excited, the associated acoustic impedance can be derived analytically and reads as [53]

$$Z'_r = -\frac{i\omega\rho h}{S}\frac{J_0(k_m r)I_1(k_m r) + J_1(k_m r)I_0(k_m r)}{J_2(k_m r)I_1(k_m r) - J_1(k_m r)I_2(k_m r)}, \tag{4.107}$$

where I_n is the modified Bessel's function of the first kind of order n, h is the thickness of the plate, and k_m and ρ are respectively the wavenumber and density of the plate, given by

$$k_m^2 = \omega\sqrt{\frac{\rho h}{D}}, \quad \text{and} \quad D = \frac{Eh^3}{12(1-\nu^2)}, \tag{4.108}$$

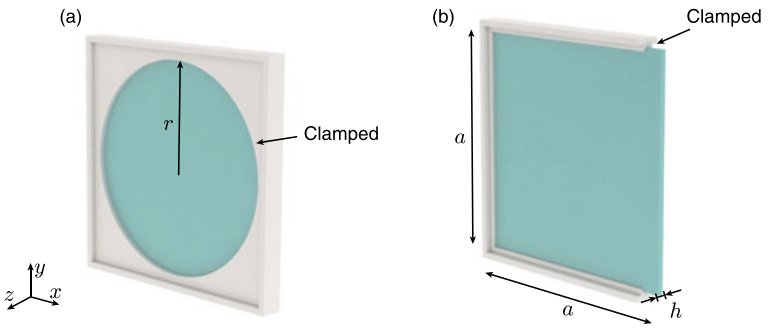

Fig. 4.14 Elastic plate resonators and the geometrical parameters used. (a) Circular elastic and (b) square clamped plates

with D is the bending stiffness (or flexural rigidity), and E and ν, the Young's modulus and Poisson's ratio of the material plate, respectively.

4.3.9.2 Approximation

Taylor expanding (4.107) at low frequencies, i.e., $k_m r \ll 1$, provides a lumped impedance model, which reads as

$$Z_r' = \frac{1}{i\omega C_p} + i\omega M_p, \tag{4.109}$$

where the compliance and the acoustic mass are [54] respectively:

$$C_p = \frac{\pi r^6}{196.51 D}, \quad M_p = 1.8830\,\frac{\rho h}{\pi r^2}. \tag{4.110}$$

The first resonance frequency is then given by the following formulae

$$f_0 = 0.4694\frac{h}{r^2}\sqrt{\frac{E}{\rho(1-\nu^2)}}. \tag{4.111}$$

Note that this model only accounts for the first resonance and, therefore, (4.109) is only valid for $f \lessapprox f_0$.

4.3.9.3 Squared Elastic Plate

The impedance of a squared clamped elastic plate, as shown in Fig. 4.14b, can be obtained assuming the system obeys the flexural wave equation which is valid for thin

elastic plates. Using separation of variables, the full expression for the impedance of a square cross-sectional elastic plate of side a is given by [55]

$$Z_r' = \left[i\omega \int_0^a \int_0^a \left(\sum_{m=1}^{\infty} \sum_{n=1}^{\infty} \frac{\int_0^a \int_0^a X_m Y_n dx dy}{D(I_1 I_2 + 2I_3 I_4 + I_5 I_6) - \rho h \omega^2 I_2 I_6} X_m Y_n \right) dx dy \right]^{-1} \tag{4.112}$$

where $X_m(x)$ and $Y_n(y)$ are the eigenfunctions describing the shape of the n-th and m-th eigenmode of the clamped plate. They both have the same form and are given by

$$X_m(x) = G\left(\frac{\lambda_m x}{a}\right) - \frac{G(\lambda_m)}{H(\lambda_m)} H\left(\frac{\lambda_m x}{a}\right), \tag{4.113}$$

$$Y_n(y) = G\left(\frac{\lambda_n y}{a}\right) - \frac{G(\lambda_n)}{H(\lambda_n)} H\left(\frac{\lambda_n y}{a}\right). \tag{4.114}$$

The functions $G(u)$ and $H(u)$ satisfy the clamped boundary conditions and are given by

$$G(u) = \cosh(u) - \cos(u), \quad H(u) = \sinh(u) - \sin(u), \tag{4.115}$$

while λ_m and λ_n satisfy

$$\cosh(\lambda)\cos(\lambda) = 1. \tag{4.116}$$

In practice, λ_m and λ_n can be found using a root-finding algorithm such as Muller's method [56].

Finally, the integrals, I_i, are given by

$$I_1 = \int_0^a X_m(x) \frac{\partial^4 X_m(x)}{\partial x^4} dx, \qquad I_2 = \int_0^a Y_n(y)^2 dy, \tag{4.117}$$

$$I_3 = \int_0^a X_m(x) \frac{\partial^2 X_m(y)}{\partial x^2} dx, \qquad I_4 = \int_0^a Y_n(y) \frac{\partial^2 Y_n(y)}{\partial x^2} dy, \tag{4.118}$$

$$I_5 = \int_0^a Y_n(y) \frac{\partial^4 Y_n(y)}{\partial x^4} dy, \qquad I_6 = \int_0^a X_m(x)^2 dx. \tag{4.119}$$

While the derivatives can be calculated analytically, the integrals must be calculated numerically, e.g., using Simpson's method.

The resonance frequencies of the n-th and m-th modes of the square clamped plate are given by

$$\omega_{m,n} = \sqrt{\frac{D(I_1 I_2 + 2I_3 I_4 + I_5 I_6)}{\rho h I_2 I_6}}. \tag{4.120}$$

Finally, note that in (4.112) the term $\int_0^a \int_0^a X_m Y_n dxdy$ vanish for $m, n = 2, 4, \ldots$, so that the even modes do not contribute to impedance: for these modes, the pressure drop at both sides of the plate is zero.

4.3.9.4 Approximation

The impedance of a square clamped plate given by (4.112) can be approximated for frequencies around and below the first resonance frequency of the plate. The lumped impedance model for the square clamped plate can be written as

$$Z_r' = \frac{1}{i\omega C_p} + i\omega M_p, \tag{4.121}$$

where the compliance and the acoustic mass are [57], respectively

$$C_p = 3.73 \times 10^{-4} \frac{a^6}{D}, \quad M_p = 2.06 \frac{\rho h}{a^2}, \tag{4.122}$$

with $D = Eh^3/12(1-\nu^2)$ the bending stiffness, and E, ν, ρ and h the Young's modulus, Poisson's ratio, density and thickness of the square plate, respectively. The first resonance frequency ω_0 of the clamped elastic square plate satisfies $\mathrm{Im}(Z_r') = 0$ and is thus given by $\omega_0 = \sqrt{1/M_p C_p}$.

4.3.10 Membranes

A clamped membrane is a thin elastic plate clamped at the boundaries under a large pre-stretch tension. As shown in Fig. 4.15a, b, the membrane behaviour arises when the tension T is much higher than the bending stiffness of the elastic plate, i.e., $T \gg D$, which is easily achieved by thin elastic plates, $h \ll \sqrt[3]{12(1-\nu^2)T/E}$, of soft materials, $\nu \to 0.5$. As in elastic plates, different geometries led to different expressions for the acoustic impedance of membranes.

4.3.10.1 Circular Membrane

Considering only the axisymmetric modes of a circular membrane of radius r and area $S = \pi r^2$, and thickness h, as depicted in Fig. 4.15a, an analytical expression can be obtained for the acoustic impedance of the clamped circular clamped membrane as

$$Z_r' = -\frac{i\omega\rho h}{S} \frac{J_0(k_m r)}{J_2(k_m r)}, \tag{4.123}$$

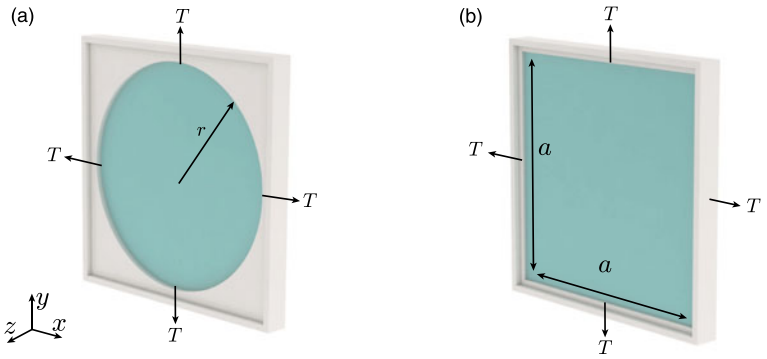

Fig. 4.15 Elastic membrane resonators and the geometrical parameters used. **a** Circular and **b** square membranes

where ρ is the material density and $k_m = \omega\sqrt{\rho/T}$ is the wavenumber in the membrane, with T the tension applied to the membrane.

4.3.10.2 Approximation

The Taylor expansion of (4.123) at the low frequencies ($k_m r \ll 1$) provides the lumped impedance model, which takes the form

$$Z_r' = \frac{i\omega\rho h}{S}\left[1 - \frac{f_0}{f}\right], \tag{4.124}$$

where the first resonance of the plate f_0 is given by the following approximation

$$f_0 = 0.38274\frac{1}{r}\sqrt{\frac{T}{\rho}}. \tag{4.125}$$

Note this model only accounts for the first resonance and, therefore, is only valid for $0 \leq f \lessapprox f_0$.

4.3.10.3 Squared Membrane

In the case of a square clamped membrane of side a and thickness h, as shown in Fig. 4.15b, the acoustic impedance can be written as [57]:

$$Z_r' = \left[i\omega a^2 \sum_{m=1}^{\infty}\sum_{n=1}^{\infty} \frac{4\left[1-(-1)^m\right]^2\left[1-(-1)^n\right]^2}{\rho h\left(\omega_{m,n}^2 - \omega^2\right)m^2 n^2 \pi^4}\right]^{-1}, \tag{4.126}$$

where ρ is the material density, m and n are the indices of the normal modes of the membrane and their corresponding resonance frequency $\omega_{m,n}$ is given by

$$\omega_{m,n} = \frac{\pi}{a}\sqrt{\frac{T}{\rho}\left(m^2 + n^2\right)}, \tag{4.127}$$

with the tension T. Note that the even modes do not contribute to the impedance because the term $[1 - (-1)^m]^2\,[1 - (-1)^n]^2$ in (4.126) vanish for $n, m = 2, 4, \ldots$, i.e., for these modes the pressure drop is zero.

4.3.10.4 Approximation

The impedance of a square clamped membrane given by (4.126) can be approximated for frequencies around or below the first resonance by

$$Z_r' = \frac{1}{i\omega C_m} + i\omega M_m, \tag{4.128}$$

where the acoustic compliance and acoustic mass are given by

$$C_m = 0.035\frac{a^6}{T}, \quad M_m = 1.44\frac{\rho h}{a^2}. \tag{4.129}$$

These coefficients are calculated from the full analytic model. Note the impedance of the membrane is independent of the material elasticity. These formulae are valid for thin clamped square membranes where the pre-stretched tension dominates over the bending stiffness, i.e., $T \gg Eh^3/12(1-\nu^2)$. The first resonance frequency of the clamped square membrane, ω_0, again satisfies $\mathrm{Im}(Z_r') = 0$ and is thus given by $\omega_0 = \sqrt{1/M_p C_p}$.

4.3.11 Infinite Elastic Vibrating Wall

A thin and unbounded elastic material of thickness h can be included in a TMM formulation as a series element given by (4.93), under the assumption that $k_l h \ll 1$, where k_l is the wavenumber associated with the longitudinal waves in the elastic material. The acoustic impedance of this thin, unbounded and elastic plate as shown in Fig. 4.16, can be written as

$$Z_r = Z_\mathrm{w} = \frac{D}{i\omega}\left(k_0^4 \sin^4\theta - k_\mathrm{w}^4\right), \tag{4.130}$$

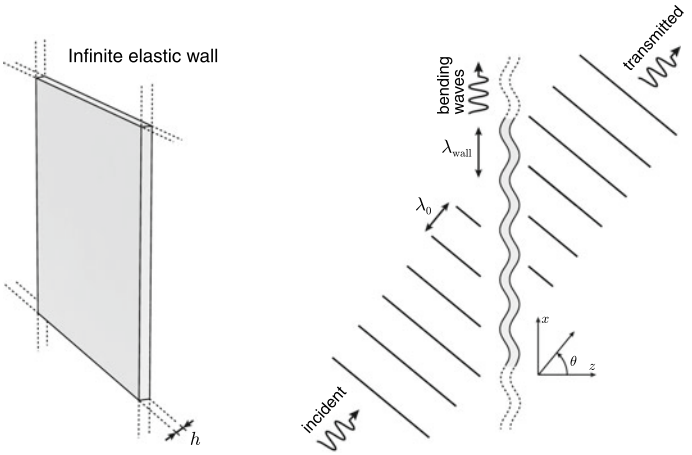

Fig. 4.16 (Left) Geometry of the unbounded elastic wall and geometrical parameters used. (Right) Scheme of the induced flexural waves at the coincidence frequency for a given angle of incidence

where θ is the incidence angle and the dispersion relation $k_{\text{w}} = \omega/c_{\text{w}}$ gives the wavenumber in the wall. The phase speed of the bending waves is $c_{\text{w}} = (\omega^2 D/m')^{1/4}$, $k_0 = \omega/c_0$ is the wavenumber of the surrounding medium with sound speed c_0, $m' = \rho h$ is the surface mass density, i.e., the mass per unit area, $D = Eh^3/12(1-\nu^2)$ is the bending stiffness of the wall and E, ν, and ρ are the Young's modulus, Poisson's ratio and density of the elastic material, respectively. Please note that the provided impedance corresponds to Z_r and not to Z_r' and holds for a thin elastic plate of infinite lateral extents.

Equation (4.130) exhibits a resonance at $k_0^4 \sin^4\theta = k_{\text{w}}^4$, i.e., when the wavenumber of the bending waves in the wall matches the transverse component of the wavenumber in the surrounding medium, as shown in Fig. 4.16. This occurs when $\lambda_0/\sin\theta = \lambda_{\text{w}}$, i.e., at the *coincidence frequency* given by

$$f_c' = \frac{c_0^2}{2\pi \sin\theta}\sqrt{\frac{m'}{D}}. \tag{4.131}$$

The lowest coincidence frequency occurs at grazing angles when $\theta = \pi/2$. We can thus define this frequency as the *critical frequency* as

$$f_c = \frac{c_0^2}{2\pi}\sqrt{\frac{m'}{D}} = f_c' \sin\theta. \tag{4.132}$$

This critical frequency only depends on the properties of the wall and the surrounding fluid. The acoustic impedance of the thin wall can then be written as a function of this critical frequency as

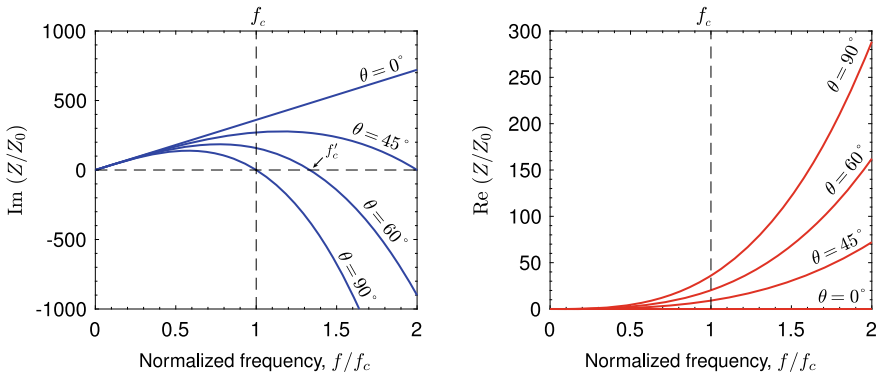

Fig. 4.17 (Left) Imaginary part of the impedance of the elastic wall as a function of the frequency normalized to the critical frequency. (Right) Corresponding real part

$$Z_{\mathrm{w}} = im'\omega \left[1 - \left(\frac{f}{f_c} \right)^2 (1 + i\eta_{\mathrm{w}}) \sin^4 \theta \right]. \tag{4.133}$$

Note that a complex bending stiffness has been introduced to account for the viscoelasticity of the solid material with $D' = D(1 + i\omega\eta_{\mathrm{w}})$, where η_{w} is the loss factor. For normal incidence or for frequencies $f \ll f_c$, the impedance reduces to $Z_{\mathrm{w}} \approx im'\omega$, i.e., only the mass of the wall contributes to the acoustic impedance.

As an example, the impedance of a $h = 1.5$-cm thick vibrating gypsum wall with $\rho = 850\,\mathrm{kg/m^3}$, $E = 4.1$ GPa, $\nu = 0.3$ and $\eta_{\mathrm{w}} = 0.1$ Pa/s, is given in Fig. 4.17. First, we can observe that the imaginary part of the impedance under normal incidence, $\theta = 0$ does not cross at zero. However, the imaginary part of the impedance vanishes for oblique incidence at some specific frequencies, i.e., at the coincidence frequencies of the wall, and thus the wall resonates. The real part of the impedance accounts for the losses of the element. At normal incidence, no loss is noticed, (4.133). At oblique incidence, the losses are activated, and they present a quadratic dependence on frequency.

4.4 Examples of Application

4.4.1 Absorption of Multilayered Porous Structure

One of the simplest configurations where the TMM has been widely used is in the modelling of absorption properties of multilayer rigidly-backed porous materials. These structures are widely used in room acoustics, as well as in automotive and aerospace applications. In most of these situations, the goal is to produce structures

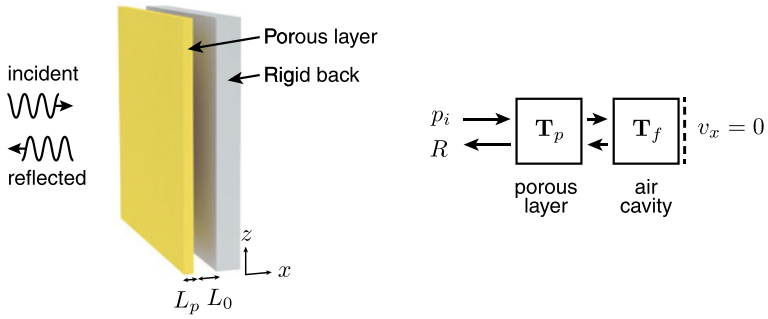

Fig. 4.18 Geometry of the configuration, composed of a porous layer with a rigidly-backed air cavity (plenum)

with high absorption coefficients. In this case, we consider that the porous material is rigidly backed, i.e., there is no transmission.

In this example we present a simple multilayer structure composed of a layer of porous material and a layer of air, i.e., an air plenum, as Fig. 4.18 shows. Note the extension of the proposed example to a higher number of layers is straightforward [12, 13].

The total transfer matrix of the system is composed of two transfer matrices, each one corresponding to the propagation in one media, that is written as

$$\mathbf{T} = \mathbf{T}_p \mathbf{T}_f, \tag{4.134}$$

where $\mathbf{T}_p$ is the transfer matrix of the porous layer of length L_p, given by (4.68), and $\mathbf{T}_f$ is the transfer matrix of the air gap of length L_0 given by (4.53). In this example, we consider a JCA model for the layer of porous material, with parameters corresponding to a mineral wool material: $\sigma = 20.6 \times 10^3$ Ns/m^4, $\alpha_\infty = 1.01$, $\phi_p = 0.98$ $\Lambda = 85$ μm, $\Lambda' = 2\Lambda$, while for the gap and the exterior media air at room temperature is considered with parameters $P_0 = 101325$ Pa, $\gamma_0 = 1.4$, $\rho_0 = 1.213$ kg/m^3, Pr $= 0.71$ $\eta_0 = 1.839 \times 10^{-5}$ Pa·s, $K_0 = \gamma_0 P_0$ Pa.

4.4.1.1 Normal Incidence

Once the full transfer matrix, $\mathbf{T}$, is obtained, the reflection and absorption coefficients are calculated using (4.48), (4.49). The total length of the multilayer structure was $L = 6$ cm. Two configurations are shown, with and without the air cavity. First, Fig. 4.19 shows the absorption of a structure calculated using a porous layer of length $L_p = 6$ cm (blue curve). In this case, the cavity of air was not included ($L_0 = 0$). Second, we show the absorption of a layer of porous material of $L_p = 3$ cm and an air cavity of $L_0 = 3$ cm (red curve). The absorbing features of the multilayer structure can be easily modelled by the TMM using a compact and fast calculation,

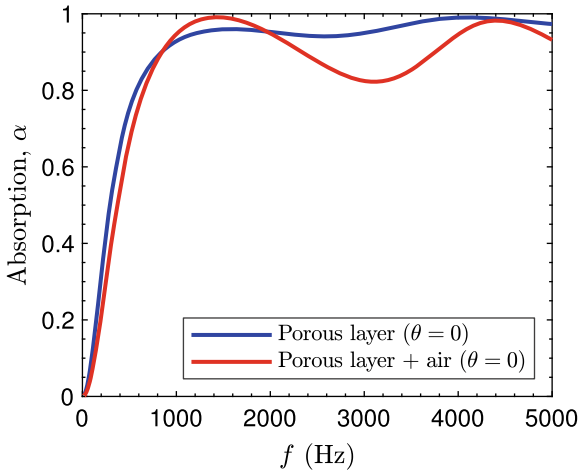

Fig. 4.19 Absorption at normal incidence angle of the rigidly-backed porous layer (black) and layer of porous material with a rigidly-backed air cavity (red)

allowing the fast optimization of the layer properties to, i.e., maximize the absorption [13]. Adding more layers with different parameters is straightforward by adding their corresponding transfer matrix terms.

4.4.1.2 Oblique Incidence

In a real situation, acoustic waves impinge the structure in more than one incidence angle. Thus, normal incidence absorption can be misleading as, in general, the absorption properties depend on the angle of incidence. We consider a plane wave with an angle of incidence θ defined with respect to the outward normal to the structure, see Fig. 4.20. Due to continuity of the transversal component of the wavevector along the interfaces, the wavenumber in the transverse direction x is the same in all media, leading to

$$k_{0,x} = k_0 \sin(\theta), \qquad k_{0,z} = \sqrt{k_0^2 - k_0^2 \sin^2(\theta)}, \tag{4.135}$$

$$k_{p,x} = k_0 \sin(\theta), \qquad k_{p,z} = \sqrt{k_p^2 - k_p^2 \sin^2(\theta)}, \tag{4.136}$$

where $k_{0,x}$ and $k_{p,x}$ are the transversal components (along x direction), and $k_{0,z}$ and $k_{p,z}$ are the normal component (along z) of the wavenumbers in the air and in the porous layer respectively, as shown in Fig. 4.20. Note that, due to symmetry considerations it is sufficient to consider only 2 components (k_z and k_z) to describe the problem: in the case of an oblique incidence with a component in the direction y, a simple rotation of the reference system can be applied to reduce the transversal wavenumber to one component.

The transfer matrix of the porous layer, $\mathbf{T}_p$, under oblique incidence is given by

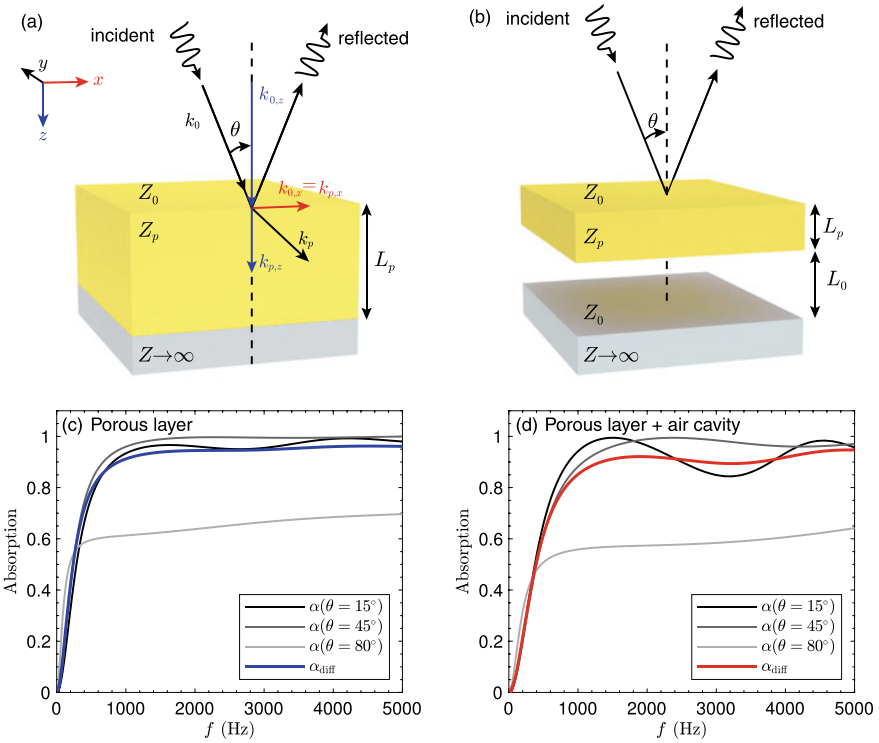

Fig. 4.20 **a** Geometry of the configuration, composed of a porous layer with rigidly-backed air cavity, **b** scheme of the transfer matrices used. **c** Absorption at of the rigidly-backed porous layer at several incidence angles (grey) and random incidence absorption (blue). **d** Absorption of layer of porous material with a air plenum and its corresponding random incidence absorption (red)

$$\mathbf{T}_p = \begin{bmatrix} \cos(k_{p,z}L_p) & iZ_p\dfrac{k_p}{k_{p,z}}\sin(k_{p,z}L_p) \\ \dfrac{i}{Z_p}\dfrac{k_{p,z}}{k_p}\sin(k_{p,z}L_p) & \cos(k_{p,z}L_p) \end{bmatrix}, \tag{4.137}$$

while the transfer matrix of the air layer, $\mathbf{T}_0$, is written as

$$\mathbf{T}_0 = \begin{bmatrix} \cos(k_{0,z}L_0) & iZ_0\dfrac{k_0}{k_{0,z}}\sin(k_{0,z}L_0) \\ \dfrac{i}{Z_0}\dfrac{k_{0,z}}{k_0}\sin(k_{0,z}L_0) & \cos(k_{0,z}L_0) \end{bmatrix}. \tag{4.138}$$

Finally, the reflection coefficient of the rigidly-backed structure under oblique incidence is obtained by setting $v_z|_{z=L} = 0$. After some algebra, it can be written as a function of the elements of the total transfer matrix given in (4.13) as

$$R(\omega,\theta)=\frac{T_{11}(\omega)\cos(\theta)-Z_0T_{21}(\omega)}{T_{11}(\omega)\cos(\theta)+Z_0T_{21}(\omega)}. \tag{4.139}$$

Then, the absorption is calculated as usual as $\alpha(\omega,\theta)=1-|R(\omega,\theta)|^2$. In addition, the specific impedance at the first interface can be calculated from the reflection coefficient as

$$Z_s(\omega,\theta)=\frac{Z_0}{\cos(\theta)}\frac{(1+R(\omega,\theta))}{(1-R(\omega,\theta))}. \tag{4.140}$$

The specific impedance at the first interface is useful to study the impedance matching of the structure with the exterior medium.

A common approach to quantify the performance of the structures under oblique incidence is to integrate the absorption for all the angles of incidence to obtain the absorption coefficient in diffuse field, α_{diff}, as [46]

$$\alpha_{\text{diff}}(\omega)=\frac{\displaystyle\int_{\theta=0}^{\theta_m}\alpha(\omega,\theta)\sin(\theta)\cos(\theta)d\theta}{\displaystyle\int_{\theta=0}^{\theta_m}\cos(\theta)\sin(\theta)d\theta}. \tag{4.141}$$

Note that for a hemispherical integration, $\theta_m=\pi/2$, this reduces to

$$\alpha_{\text{diff}}(\omega)=\int_{\theta=0}^{\pi/2}\alpha(\omega,\theta)\sin(2\theta)d\theta, \tag{4.142}$$

known as the Paris' formula. This coefficient is closely related to the measurement of sound absorption under random incidence in a reverberant chamber following the standardized acoustic test ISO 354:2003 [58]. Note the experimental test should differ from the calculations due to many factors, including a non-diffuse field in the reverberant chamber or the absorption at the boundaries of the finite-dimension material [59]. Figure 4.20c–d show the predicted absorption for various angles of incidence for both configurations. The absorption coefficient in diffuse field is also shown, where it can be observed that under random incidence the absorption curve is smoothed.

4.4.2 Noise Transmission Through a Double Wall

Other interesting problem that has been widely solved using the TMM in the literature is the transmission of acoustic waves travelling through multiple elastic walls. This concerns the classical problem of noise transmission in building acoustics for sound-proofing, as well as sound transmission in automotive and aerospace applications [60]. In the following, we present the solution of a classical example of a double-

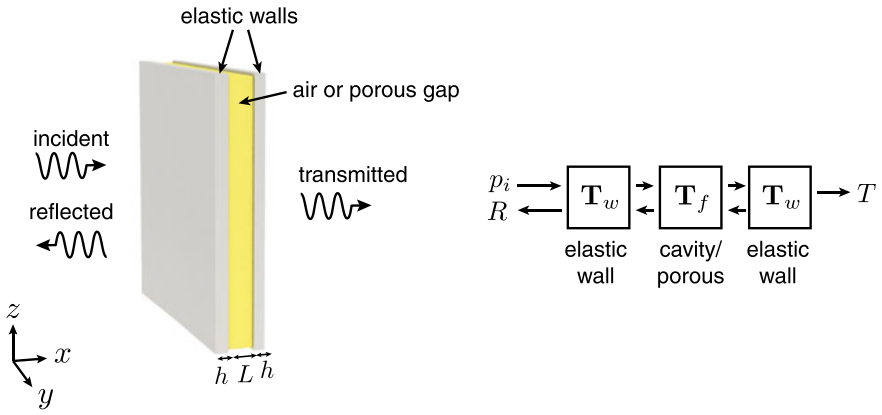

Fig. 4.21 Geometry of the configuration, composed of a double elastic wall separated by a cavity and scheme of the transfer matrices used

wall sound proofing system composed of two layers of gypsum board separated a distance L, with an air cavity between the walls, as shown in Fig. 4.21.

In this case, the total transfer matrix is given by

$$\mathbf{T} = \mathbf{T}_w^{[1]} \mathbf{T}_f \mathbf{T}_w^{[2]}, \tag{4.143}$$

where $\mathbf{T}_w^{[1,2]}$ are the transfer matrices of the gypsum boards given by (4.133), and $\mathbf{T}_f$ is the transfer matrix of the air cavity given by (4.53). The total transfer matrix under oblique incidence then

$$\mathbf{T} = \begin{bmatrix} 1 & Z_1 \\ 0 & 1 \end{bmatrix} \begin{bmatrix} \cos(k_{0,z}L) & iZ_0 \dfrac{k_0}{k_{0,z}} \sin(k_{0,z}L) \\ \dfrac{i}{Z_0} \dfrac{k_{0,z}}{k_0} \sin(k_{0,z}L) & \cos(k_{0,z}L) \end{bmatrix} \begin{bmatrix} 1 & Z_2 \\ 0 & 1 \end{bmatrix}, \tag{4.144}$$

where the perpendicular and transverse wavenumbers are given by

$$k_{0,z} = \sqrt{k_0^2 - k_0^2 \sin^2(\theta)} \quad \text{and} \quad k_{0,x} = k_0 \sin(\theta), \tag{4.145}$$

and Z_1 and Z_2 are the impedances of the infinite elastic walls given by (4.133). Once the total transfer matrix is calculated, we can obtain the transmission coefficient T using (4.37). Then, we can represent the transmission loss in logarithmic scale as

$$TL = -10 \log_{10} |T|^2, \tag{4.146}$$

which is useful to quantify the soundproofing performance of structures.

4.4.2.1 Normal Incidence

For normal incidence, $\theta = 0$, then $k_{0,z} = k_0$. We can calculate the total transfer matrix from (4.144), and then the transmission coefficient using (4.37) to obtain

$$T = \frac{1}{\left(1 + \dfrac{Z_1 + Z_2}{2Z_0}\right)\cos(k_0 L) + i\left(1 + \dfrac{Z_1 + Z_2}{2Z_0} + \dfrac{Z_1 Z_2}{2Z_0^2}\right)\sin(k_0 L)}. \quad (4.147)$$

For normal incidence (4.133) leads to $Z_1 \approx i\omega m_1'$ and $Z_2 \approx i\omega m_2'$, i.e., only the mass of each wall contributes to their impedance.

We show an example for normal incidence using a double-wall composed of two identical gypsum panels of $h = 1.5$ cm thickness, separated by a distance $L = 5$ cm with a density of $\rho = 850$ kg/m^3, Young modulus of $E = 4.1$ GPa, Poison ratio of $\nu = 0.3$ and losses modelled by $\eta = 0.05$. Air is assumed to fill the cavity. Figure 4.22 shows that (4.147) gives the same solution as the numerical evaluation of the transfer matrix (4.144). Moreover, approximate expressions for each regime (dashed lines), can be obtained, as well as the transition frequencies.

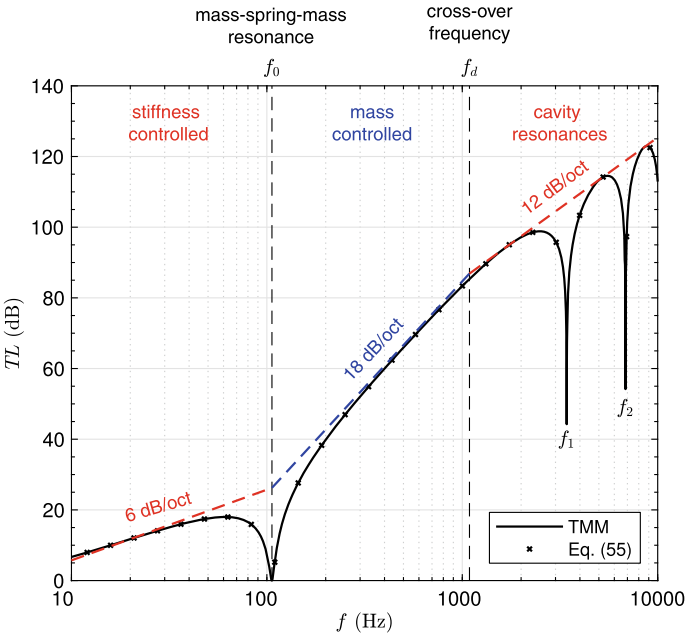

Fig. 4.22 Transmission loss (TL) at normal incidence angle using an air cavity (black) and using (4.147). Approximate solution are marked in dashed lines

4.4.2.2 Low Frequency Approximation

For low frequencies, $k_0 L \ll 1$, we can approximate $\sin(k_0 L) \approx k_0 L$ and $\cos(k_0 L) \approx 1 - k_0^2 L^2/2$. Then, neglecting high order terms we obtain

$$TL \approx 20 \log_{10} \left(\frac{\omega(m_1 + m_2)}{2Z_0} \right), \quad \text{for} \quad f < f_0. \tag{4.148}$$

This frequency regime corresponds to the well-known *mass law*: the double-wall system behaves as a single wall with total surface mass $(m'_1 + m'_2)$. Thus, the transmission decreases with the square of the frequency, i.e., the transmission loss increases 6 dB/octave.

This expression is valid for frequencies up to the double-wall resonance frequency, f_0, given by

$$f_0 = \frac{1}{2\pi} \sqrt{\frac{K_0}{L} \left(\frac{1}{m'_1} + \frac{1}{m'_2} \right)}. \tag{4.149}$$

At this particular frequency the double-wall resonates as a mass-spring-mass system, where walls contribute to both masses (m'_1 and m'_2) and the bulk modulus of the inner cavity ($K_0 = \rho_0 c_0^2$) contributes to the stiffness of the equivalent spring. At this resonance frequency a peak of transmission is observed, producing a deep dip in the transmission loss.

4.4.2.3 Medium Frequency Approximation

For intermediate frequencies up to $k_0 L \approx 1$, the transmission loss of the system can be simplified to

$$TL \approx 20 \log_{10} \left(\frac{\omega^3 m'_1 m'_2 L}{2\rho_0^2 c_0^3} \right), \quad \text{for} \quad f_0 < f < f_d. \tag{4.150}$$

In this regime the transmission increases with the sixth power of the frequency, i.e., the transmission loss increases with 18 dB/octave. Here, the transmission loss depends on the product of the masses and the separation of the panels, i.e., the transmission loss is the addition of the insulation of both walls plus an additional term as $TL \approx TL_1 + TL_2 + 20 \log_{10}(2k_0 L)$, where $TL_1 = 20 \log_{10}(\omega m'_1/2Z_0)$ and $TL_2 = 20 \log_{10}(\omega m'_2/2Z_0)$ are the transmission losses of both independent walls, respectively. Note the soundproofing performance of the double-wall in this regime is greatly improved if compared with the performance of a panel with equivalent mass.

This expression is valid for frequencies up to $k_0 L \approx 1$, leading to a cut-off frequency of

$$f_d = \frac{c_0}{2\pi L}. \tag{4.151}$$

Above this frequency the resonances of the inner air cavity start to dominate.

4.4.2.4 High Frequency Regime

Above f_d, the cavity between the two walls shows several resonances given by $k_0 L = n\pi$, where $n = 1, 2, 3, ...$ Thus, the resonance frequencies are

$$f_n = n\frac{c_0}{2L}. \tag{4.152}$$

At each resonance frequency a peak of transmission is produced, leading to a dip in the transmission loss. The overall TL in this regime, neglecting the dips given by the resonances, can be approximated by

$$TL \approx 20\log_{10}\left(\frac{\omega^2 m_1' m_2'}{2Z_0^2}\right), \quad \text{for} \quad f_d < f. \tag{4.153}$$

In this regime the transmission decreases with the fourth power of the frequency, i.e., the transmission loss increases with a slope of 12 dB/octave. This is roughly equivalent to $TL \approx TL_1 + TL_2 + 6$ dB.

4.4.2.5 Oblique Incidence

As occurs with the reflection problem, the transmission at normal incidence does not describe a real situation where acoustic waves will impinge the walls at more than one incidence angle. In addition, for each oblique incidence angle there exist a frequency at which the corresponding wavelength of air matches the wavelength of the bending waves travelling trough the infinite wall. Then, the impedance of each wall should introduce a contribution modelling these phenomena, as shown in (4.133).

Under oblique incidence, the transmission coefficient is calculated as

$$T(\omega, \theta) = \frac{2}{T_{11} + T_{12}\cos(\theta)/Z_0 + T_{22} + T_{21}Z_0/\cos(\theta)}. \tag{4.154}$$

In addition, manipulating the total transfer matrix we can obtain the characteristic frequencies under oblique incidence as

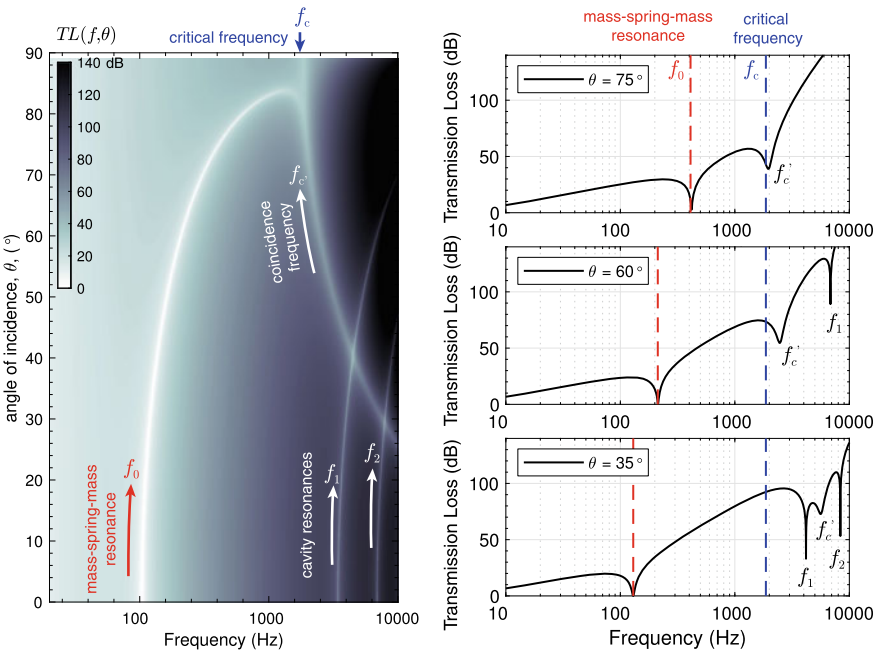

Fig. 4.23 (left) Transmission loss as a function of the frequency and the angle of incidence. The white dips mark the existence of resonance modes that led to transmitted energy. (right-bottom) Transmission loss near the normal, at $\theta = 35°$. The effect of the coincidence mode is visible at frequency f_c'. Cavity resonances are also clearly visible at f_1 and f_2. (Right-center) Transmission loss at $\theta = 60°$. The effect of the coincidence mode is visible at frequency f_c', cavity resonances have increased their frequency. (Right-top) Transmission loss near the grazing angle, at $\theta = 75°$. The effect of the coincidence mode dominates and its frequency almost match the critical frequency. The effect of cavity resonances in the transmission loss is negligible

$$\text{Mass-spring-mass resonance:} \qquad f_0(\theta) = \frac{1}{2\pi\cos(\theta)}\sqrt{\frac{K_0}{L}\left(\frac{1}{m_1'} + \frac{1}{m_2'}\right)},$$

$$\text{Coincidence frequency:} \qquad f_c'(\theta) = \frac{f_c}{\sin^2(\theta)},$$

$$\text{Cavity resonances:} \qquad f_n(\theta) = n\frac{c_0}{2L\cos(\theta)} \text{ with } n = 1, 2, 3, \ldots$$

where f_c is the critical frequency given by (4.132), i.e., the coincidence frequency for an incidence angle of $\theta = \pi/2$.

Figure 4.23 shows the transmission loss as a function of the incidence angle and frequency. We can observe that the overall transmission loss is reduced when the incident wavefront is tilted, mainly caused by the existence of a resonant transmission due to the coincidence effect. The mass-spring-mass resonance also shifts in

frequency causing a reduction of the transmission loss in the low frequency regime. The cavity modes are shifted-up in frequency.

To quantify the overall transmission loss in realistic situation including random incidence, it is useful to integrate the angle-dependent transmission of the single to obtain the diffuse-field transmission loss as

$$TL_{\text{diff}}(\omega) = -10\log_{10}\frac{\displaystyle\int_{\theta=0}^{\theta_m} T(\omega,\theta)\cos(\theta)\sin(\theta)d\theta}{\displaystyle\int_{\theta=0}^{\theta_m}\cos(\theta)\sin(\theta)d\theta}. \tag{4.155}$$

where θ_m is usually in the range from 80° to 90°.

This coefficient is related (but not equivalent) to the standardized test defined in the ASTM E90-09 [61] to experimentally evaluate the insertion loss of a panel in a transmission chamber. Note that, if $\theta_m = \pi/2$, then

$$TL_{\text{diff}}(\omega) = -10\log_{10}\int_{\theta=0}^{\pi/2} T(\omega,\theta)\sin(2\theta)d\theta, \tag{4.156}$$

in analogy with the Paris' formula for the diffuse-field absorption given by (4.142).

4.4.2.6 Porous Layer in the Cavity

A common solution to increase the transmission loss at the cavity resonances is to add a layer of porous material in the cavity. Thus, we can modify the total transfer matrix as

$$\mathbf{T} = \mathbf{T}_w^{[1]}\mathbf{T}_f\mathbf{T}_p\mathbf{T}_f\mathbf{T}_w^{[2]}, \tag{4.157}$$

where $\mathbf{T}_p$ is the transfer matrix of the porous material given by (4.68) and $\mathbf{T}_f$ is the transfer matrix of the air gap between the porous material and the walls, given by (4.53). We consider a cavity of 5 cm, with a layer of porous material of thickness $L_p = 4$ cm, modelled using the JCA model and using a static air flow resistivity of $\sigma = 9958$ Ns/m^4, a high frequency limit of the tortuosity $\alpha_\infty = 1.03$, and open porosity of $\phi_p = 0.982$ a viscous characteristic length of $\Lambda = 203$ μm and a thermal characteristic length of $\Lambda' = 2\Lambda$ μm. Therefore, the air gap at each side of the porous layer is $L_0 = 0.5$ cm.

The transmission loss of the system is shown in Fig. 4.24. Note that, in this case, instead of obtaining an explicit analytical form like (4.147), it is more straightforward to directly evaluate numerically the transfer matrix of each element in (4.157). First, for normal incidence we can see that at the cavity resonances (f_1, f_2, ...) the transmission loss is greatly increased due to the damping of the purely acoustic modes propagating in the air between the layers. This is the principal benefit of

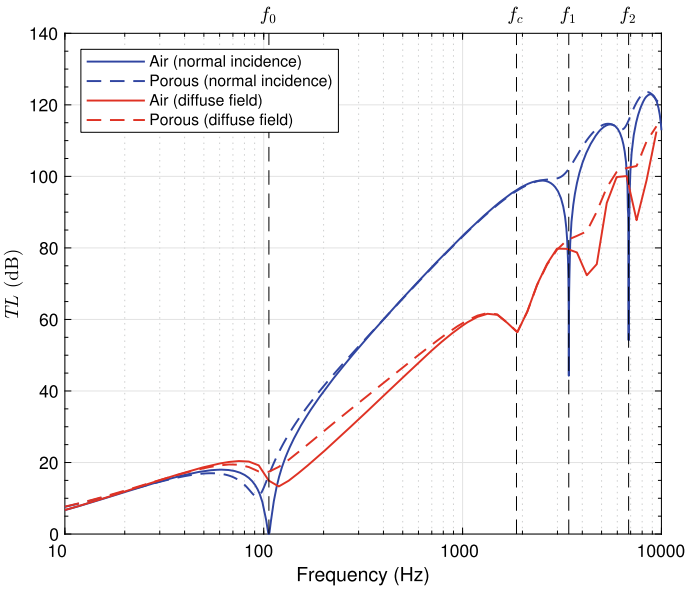

Fig. 4.24 Transmission loss of the double-wall system without (continuous) and with (dashed) the porous absorber. (Blue) normal incidence, (red) diffuse field

using a porous material inside the cavity. At the mass-spring-mass resonance (f_0) the transmission is not longer perfect but the value of the TL remains low.

On the other hand, for diffuse field calculations, we can see that the transmission loss is greatly reduced as compared with the normal incidence. This is mainly caused by the coincidence effect that sweeps an almost perfectly transmitted mode all over the spectra down to the critical frequency, as shown previously in Fig. 4.23. When the layer of porous material is introduced, its effect is clearly visible at high frequencies as it mainly attenuates the modes in the cavity. However, the contribution of the porous material to reduce the transmission of the coincidence effect is very low, and, therefore, the TL value at the critical frequency (f_c) remains low.

Note that, using the TMM the inclusion of more elements and layers to the system is straightforward. However, in a realistic situation in building acoustics other important phenomena should be considered: the transmission by the flanks, stubs and supporting systems, the finite size of the elastic walls and many other vibro-acoustic effects [60].

4.4.3 Phononic Crystals

We present the analysis of 1D periodic structures and metamaterials using the TMM. An acoustic periodic media is an arrangement of acoustic elements, unit cells, whose

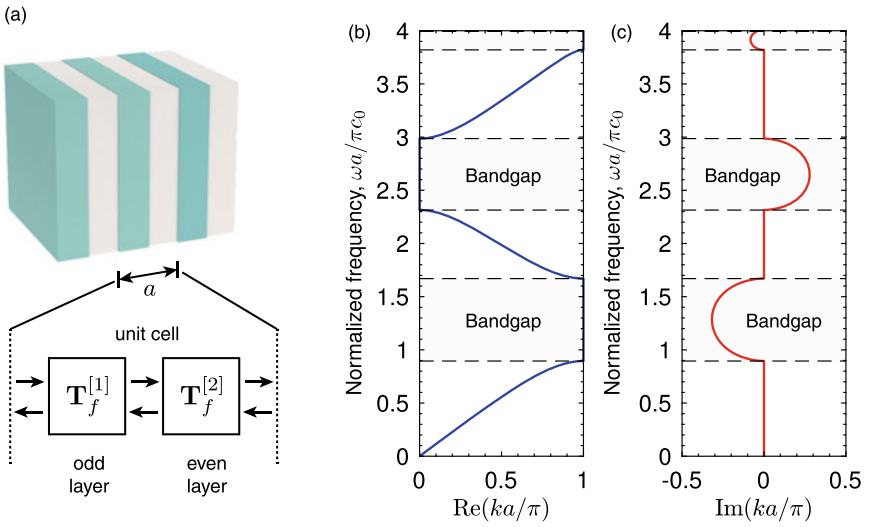

Fig. 4.25 **a** Geometry of a phononic crystal made of alternating layers of two materials. **b–c** Dispersion relations obtained for the phononic crystal, real and imaginary part of the wavenumber, respectively. Bandgap regions are shaded

structure is repeated in space. A simple example of such media is a periodic-multilayer structure composed of two fluid layers with alternating properties, as shown in Fig. 4.25a, also named a phononic crystal in analogy with photonic crystals in optics.

The total transfer matrix of the unit cell considered in this problem, $\mathbf{T}_{\text{u.c.}}$, is given by the product of the transfer matrices of each layer as

$$\mathbf{T}_{\text{u.c.}} = \mathbf{T}_f^{[1]}\mathbf{T}_f^{[2]}, \tag{4.158}$$

where $\mathbf{T}_f^{[1]}$ is the transfer matrix of the first fluid and $\mathbf{T}_f^{[2]}$ is the transfer matrix of the second fluid, both given by (4.53). Here, we consider a unit cell of total length a, where the length of each layer is a_1 and a_2 respectively. Due to the periodicity of the structure, it is sufficient to analyse a single unit cell to obtain the dispersion relations, as well as the transmission and reflection properties.

When analysing period structures it is important to note that their dispersion relations are defined for infinite period structures, while to obtain their reflection and transmission properties these structures must be bounded in space, i.e., the scattering properties depend on the number of unit cells considered.

4.4.3.1 Derivation of the Dispersion Relation of a 1D Multilayer System

We consider two fluids with different wavenumbers and impedances, given by $k_1 = \omega/c_1$, $k_2 = \omega/c_2$ and $Z_1 = \rho_1 c_1$ and $Z_2 = \rho_2 c_2$, where ρ_1 and ρ_2 are the density and c_1 and c_2 the sound speed of each fluid. The periodicity of the system is $a = a_1 + a_2$. Then, the transfer matrices of both fluids are given by (4.53), respectively

$$\mathbf{T}_f^{[1]} = \begin{bmatrix} T_{11}^{[1]} & T_{12}^{[1]} \\ T_{21}^{[1]} & T_{22}^{[1]} \end{bmatrix} = \begin{bmatrix} \cos(k_1 a_1) & iZ_1 \sin(k_1 a_1) \\ i\dfrac{1}{Z_1} \sin(k_1 a_1) & \cos(k_1 a_1) \end{bmatrix} \tag{4.159}$$

and

$$\mathbf{T}_f^{[2]} = \begin{bmatrix} T_{11}^{[2]} & T_{12}^{[2]} \\ T_{21}^{[2]} & T_{22}^{[2]} \end{bmatrix} = \begin{bmatrix} \cos(k_2 a_2) & iZ_2 \sin(k_2 a_2) \\ i\dfrac{1}{Z_2} \sin(k_2 a_2) & \cos(k_2 a_2) \end{bmatrix}. \tag{4.160}$$

In acoustics, for these periodic systems, the pressure and velocities accomplish the Bloch-Floquet theorem providing the following relation between the boundaries of the unit cell

$$\begin{bmatrix} p \\ v_x \end{bmatrix}_{x=0} = \mathbf{T}_{\text{u.c.}} \begin{bmatrix} p \\ v_x \end{bmatrix}_{x=a} = \begin{bmatrix} T_{11} & T_{12} \\ T_{21} & T_{22} \end{bmatrix} \begin{bmatrix} e^{-ika} p \\ e^{-ika} v_x \end{bmatrix}_{x=0}. \tag{4.161}$$

Rearranging this equation we obtain

$$\left(\begin{bmatrix} T_{11} & T_{12} \\ T_{21} & T_{22} \end{bmatrix} - \begin{bmatrix} e^{ika} & 0 \\ 0 & e^{ika} \end{bmatrix} \right) \begin{bmatrix} p \\ v_x \end{bmatrix}_{x=a} = 0. \tag{4.162}$$

Defining $\Lambda = e^{ika}$, this system only has solution if

$$\left| \begin{bmatrix} T_{11} - \Lambda & T_{12} \\ T_{21} & T_{22} - \Lambda \end{bmatrix} \right| = 0. \tag{4.163}$$

By using the condition of reciprocity: $T_{11}T_{22} - T_{12}T_{21} = 1$, we obtain the following dispersion relation

$$\cos(k_e a) = \frac{T_{11} + T_{22}}{2} = \frac{\text{Tr}(\mathbf{T}_{\text{u.c.}})}{2}. \tag{4.164}$$

Thus, by solving the matrix product between (4.159) and (4.160) we obtain the coefficients of the total transfer matrix as

$$T_{11} = \cos(k_1 a_1)\cos(k_2 a_2) - \frac{Z_1}{Z_2}\sin(k_1 a_1)\sin(k_2 a_2), \tag{4.165}$$

$$T_{12} = iZ_1\cos(k_2 a_2)\sin(k_1 a_1) + iZ_2\cos(k_1 a_1)\sin(k_2 a_2), \tag{4.166}$$

$$T_{21} = \frac{i}{Z_1}\sin(k_1 a_1)\cos(k_2 a_2) + \frac{i}{Z_2}\cos(k_1 a_1)\sin(k_2 a_2), \tag{4.167}$$

$$T_{22} = \cos(k_1 a_1)\cos(k_2 a_2) - \frac{Z_2}{Z_1}\sin(k_1 a_1)\sin(k_2 a_2). \tag{4.168}$$

On the one hand, the effective wavenumber can be calculated by the terms T_{11} and T_{22} using (4.15). Then, the effective wavenumber is given by

$$k_e = \frac{1}{L}\cos^{-1}\left[\cos(k_1 a_1)\cos(k_2 a_2) - \frac{Z_1^2 + Z_2^2}{2Z_1 Z_2}\sin(k_1 a_1)\sin(k_2 a_2)\right]. \tag{4.169}$$

On the other hand, the effective impedance, given by (4.16), can be obtained as $Z_e = \sqrt{T_{12}/T_{21}}$. Then we obtain

$$Z_e = \sqrt{\frac{Z_1^2 Z_2\cos(k_2 a_2)\sin(k_1 a_1) + Z_2^2 Z_1\cos(k_1 a_1)\sin(k_2 a_2)}{Z_2\cos(k_2 a_2)\sin(k_1 a_1) + Z_1\cos(k_1 a_1)\sin(k_2 a_2)}}. \tag{4.170}$$

Using these expressions the effective mass density, ρ_e, and bulk modulus, K_e, of the multilayer system are

$$\rho_e = \frac{Z_e k_e}{\omega} \quad \text{and} \quad K_e = \frac{Z_e \omega}{k_e}. \tag{4.171}$$

Note that, due to periodicity, the wavenumber is obtained only in the first Brillouin zone. However, for the calculations of the effective parameters ρ_e, K_e, a proper unwrap of the wavenumber is required.

Figure 4.25b–c show the dispersion relation of the system. First, we can see that the system is highly dispersive and the wavenumber does not depend linearly on frequency: the phase and group speeds strongly depend on frequency. Second, we can see that for certain frequency bands the wavenumber becomes imaginary. The waves that propagate in these frequency bands are evanescent, therefore, these frequency bands are called bandgaps, as explained in detail in Chaps. 1–3.

4.4.3.2 Transmission and Reflection of Bounded Phononic Crystals

The fact that waves propagating in bandgap frequencies are evanescent does not imply that energy cannot propagate in a phononic crystal. In fact, for bounded (finite) structures some amount of energy penetrates and, therefore, some acoustic transmission is expected.

For a finite phononic crystal of N unit cells the total transfer matrix is

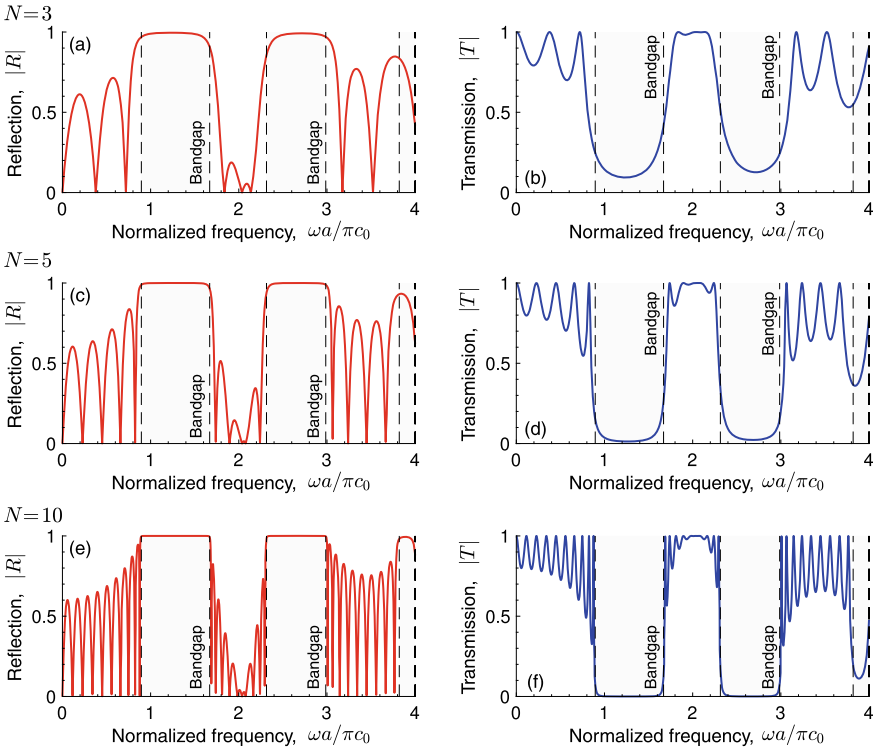

Fig. 4.26 **a**, **c**, **e** Reflection and **b**, **d**, **f** transmission coefficients of a phononic crystal of $N = 3, 5$ and 10 unit cells

$$\mathbf{T} = \mathbf{T}_{\text{u.c.}}^{N}, \tag{4.172}$$

where $\mathbf{T}_{\text{u.c.}}$ is the total transfer matrix given by (4.158).

Figure 4.26 shows the reflection and transmission coefficients of the finite phononic crystal using $N = 3, 5$ and 10 unit cells. We can see that, first, in the propagating bands there exist some peaks of transmission. In particular for frequencies $\omega a/\pi c_0 < 1$ there exist $N - 1$ peaks (neglecting the peak 0 Hz) of transmission corresponding to the Fabry-Pérot resonances of the bounded system. Obviously, at each peak of transmission the reflection vanishes as the considered system here is conservative. However, at the frequency bands corresponding to bandgap regions, the transmission drops. The energy is then strongly reflected by the structure by the constructive interference in the backward direction corresponding to the Bragg resonance.

As more unit cells are considered, the number of resonances increases accordingly: the filtering effect of the band-gap is more evident and the value of the transmission inside it decreases. However, in a finite structure without intrinsic looses some portion of the energy will always be transmitted.

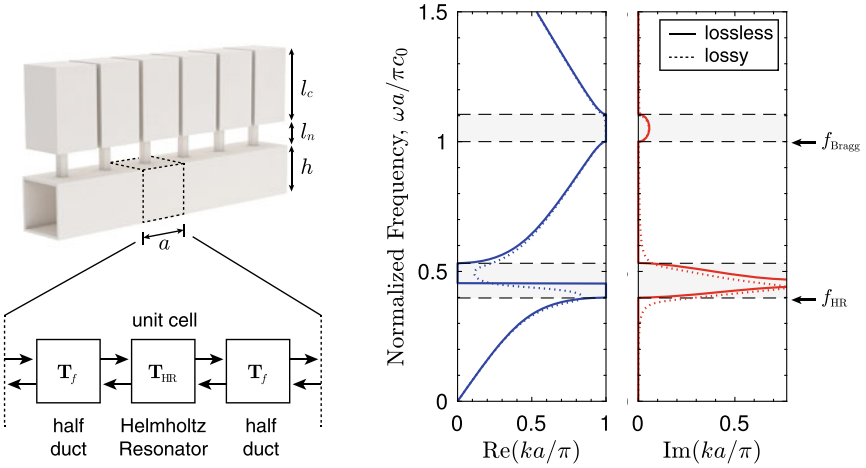

Fig. 4.27 Geometry of the negative bulk-modulus metamaterial composed of a waveguide loaded with an array of HR. Dispersion relations of the system, real and imaginary part of the wavenumber, respectively. Bandgaps are marked in shaded areas

4.4.4 Metamaterial Modelling Using TMM

The transfer matrix method has been applied to model acoustic waves propagating in locally resonant structures. Here, we show two examples, a negative bulk-modulus metamaterial made of a waveguide loaded with HR, and a negative mass-density metamaterial made of a waveguide with embedded elastic plates.

4.4.4.1 Negative Bulk Modulus Metamaterial: Waveguide Loaded with HRs

First, we show the model of a locally-resonant metamaterial composed of a waveguide loaded with HR, as shown in Fig. 4.27. The total transfer matrix of the unit cell is given by

$$\mathbf{T}_{\text{u.c.}} = \mathbf{T}_f \mathbf{T}_{\text{HR}} \mathbf{T}_f, \tag{4.173}$$

where $\mathbf{T}_f$ is the transfer matrix of the waveguide of length $a/2$ given by (4.53), and $\mathbf{T}_{\text{HR}}$ is the transfer matrix of the HR loaded in parallel, given by (4.90). Therefore, the transfer matrix of the unit cell is

$$\mathbf{T}_{\text{u.c.}} = \begin{bmatrix} \cos(k_f a') & iZ'_f \sin(k_f a') \\ i\dfrac{1}{Z'_f}\sin(k_f a') & \cos(k_f a') \end{bmatrix} \begin{bmatrix} 1 & 0 \\ \dfrac{1}{Z'_r} & 1 \end{bmatrix} \begin{bmatrix} \cos(k_f a') & iZ'_f \sin(k_f a') \\ i\dfrac{1}{Z'_f}\sin(k_f a') & \cos(k_f a') \end{bmatrix},$$

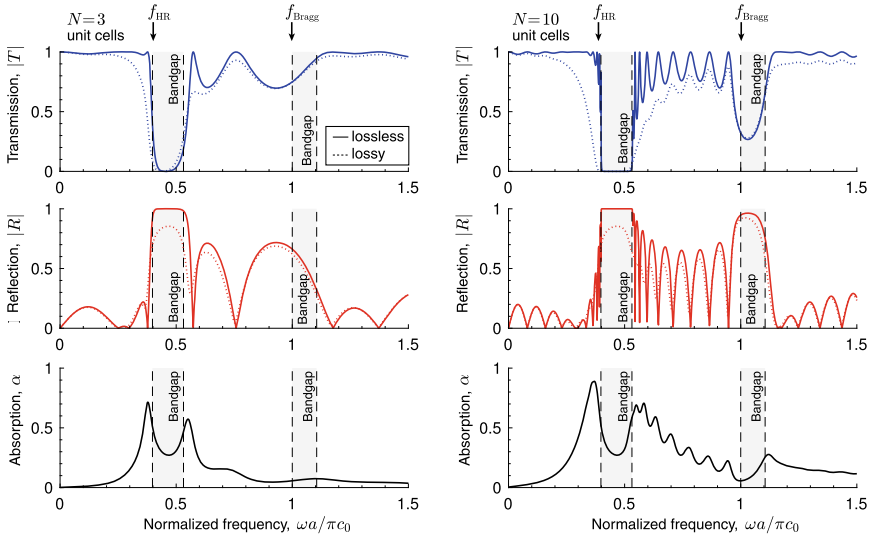

Fig. 4.28 Scattering of a negative bulk-modulus metamaterial composed of (left column) $N = 3$ unit cells and (right column) $N = 10$ unit cells. (Top row) transmission, (center row) reflection and (bottom row) absorption

where $a' = a/2$. For this example, we use a squared cross-section waveguide loaded by an array of HR, where the neck and cavity of the HR are also rectangular. Substituting (4.3.7) in (4.90), and evaluating (4.173), we can obtain the elements $T_{i,j}$ of the transfer matrix. Then, we can calculate the dispersion relations of the system by using (4.15).

Figure 4.27 shows the real and imaginary part of the wavenumber. We can see that strong dispersion is generated when the HRs are loaded in the waveguide. Bandgaps are also observed. In the example shown here, the first bandgap appears just above the resonance frequency of the HR. We can see that just in the limits of the bandgap strong dispersion is produced. Moreover, at $\omega a/\pi c_0 = 1$ a second bandgap is generated. This bandgap corresponds to the Bragg's resonance and is produced by the multiple scattering of the waves due to periodicity. Interestingly, by using the effective parameters of the duct we can include the thermoviscous losses. Obtaining an expression for the wavenumber including thermoviscous losses is straightforward but the expressions will be too much complex. Instead, in practice we simply evaluate the total transfer matrix numerically, as shown in Fig. 4.27. Note that, when introducing thermoviscous losses the dispersion relations are modified: in general, the wavenumber becomes complex in propagating bands and the strongly-dispersive flat propagating bands are smoothed.

Once the metamaterial is bounded we can obtain the reflection, transmission and absorption properties. To calculate the transmission, the reflection and the absorption of a structure with N unit cells we first evaluate the total transfer matrix as

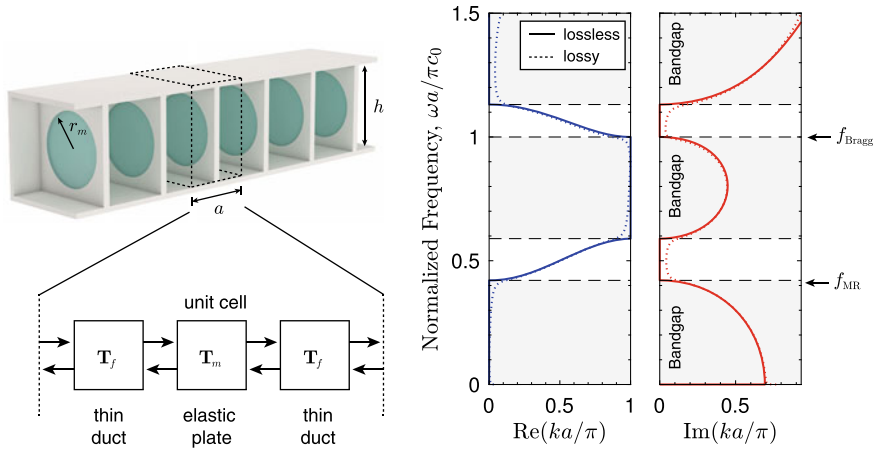

Fig. 4.29 (left) Scheme of the negative mass-density metamaterial with thin circular elastic plates. Dispersion relation of the system, (center) real and (right) imaginary part of the wavenumber. Bandgaps are marked in shaded areas

$$\mathbf{T} = \mathbf{T}_{\text{u.c.}}^{N}, \tag{4.174}$$

where $\mathbf{T}_{\text{u.c.}}$ is the total transfer matrix given by (4.173). Then, (4.37)–(4.43) are used. Figure 4.28 shows the scattering properties of the metamaterial using $N = 3$ and $N = 10$ unit cells. We can see that waves with frequencies in the range of the bandgap cannot easily propagate through the material. In the rest of the cases the structure is almost transparent to sound, specially at the Fabry-Pérot resonances of the structure. Note that the bandgap generated by the resonance introduces far more attenuation than the one caused by Bragg scattering. In addition, by adding more unit cells to the structure this effect becomes more evident. Finally, when losses are taken into account, absorption is produced mainly at the resonances of the structure. Absorption will be studied in detail in Chap. 5.

Finally, note that TMM also allows the calculation of non-periodic metamaterials based on this topology e.g., waveguides loaded by resonators of different geometry. In this case, the $\mathbf{T}$-matrix of each unit must be calculated and, using (4.13), the total transfer matrix is obtained as the product of all matrices [28].

4.4.4.2 Negative Mass-Density Metamaterial: Waveguide with Thin Plates

In the same way, we can design a metamaterial composed of a waveguide with an embedded array of thin elastic clamped plates, as shown in Fig. 4.29. These materials present negative mass-density effective parameters.

The total transfer matrix of the unit cell is given by

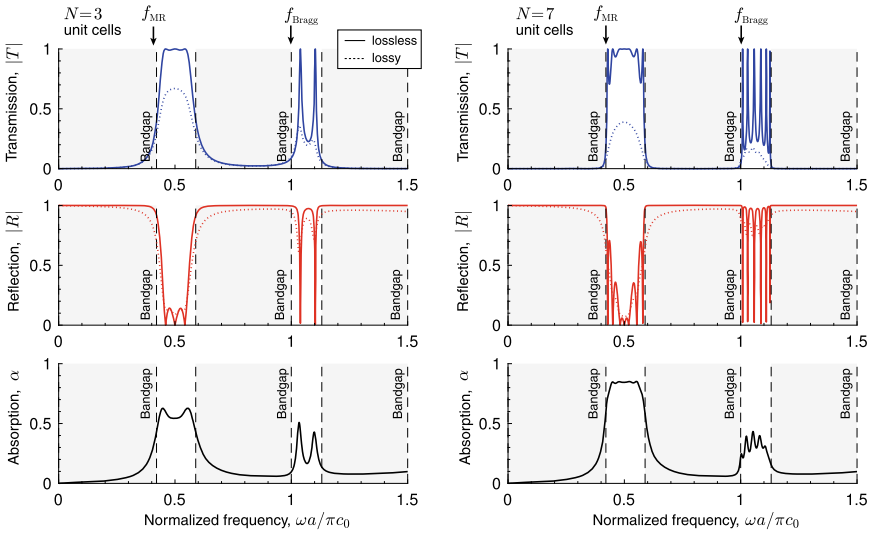

Fig. 4.30 Scattering of a negative mass-density metamaterial composed of (left column) $N = 3$ unit cells and (right column) $N = 7$ unit cells. (Top row) transmission, (center row) reflection and (bottom row) absorption

$$\mathbf{T}_{\text{u.c.}} = \mathbf{T}_f \mathbf{T}_{\text{PR}} \mathbf{T}_f, \tag{4.175}$$

where $\mathbf{T}_f$ is the transfer matrix of the waveguide of length $a/2$ given by (4.53), and $\mathbf{T}_{\text{PR}}$ is the transfer matrix of the plate resonator embedded in series, given by (4.93). Therefore, the transfer matrix of the unit cell is

$$\mathbf{T}_{\text{u.c.}} = \begin{bmatrix} \cos(k_f a') & i Z'_f \sin(k_f a') \\ i \dfrac{1}{Z'_f} \sin(k_f a') & \cos(k_f a') \end{bmatrix} \begin{bmatrix} 1 & Z'_r \\ 0 & 1 \end{bmatrix} \begin{bmatrix} \cos(k_f a') & i Z'_f \sin(k_f a') \\ i \dfrac{1}{Z'_f} \sin(k_f a') & \cos(k_f a') \end{bmatrix},$$

where $a' = a/2$. For this example, we use a squared cross-section waveguide loaded by an array of circular thin plates. Substituting (4.123) in (4.93), and evaluating (4.175), we can obtain the elements $T_{i,j}$ of the transfer matrix. Then, we can calculate the dispersion relations of the system by using (4.15).

The typical dispersion relation of this kind of system is shown in Fig. 4.29. We can see that, contrary to the previous case, waves in the low-frequency regime cannot propagate. However, above the resonance of the plates we observe that the wavenumber becomes real. In addition, a secondary bandgap is observed below Bragg frequency. Note when looses are introduced waves are damped in the propagation band and bandgap limits smooth.

The scattering properties of a system using $N = 3$ and $N = 7$ membranes are shown in Fig. 4.30. First, we can see that even for a system with few resonating elements the transmission of waves for frequencies below the resonance frequency

of the membrane is very low, as shown in Fig. 4.30 (top). Only waves corresponding to the collective modes of the set of membranes can propagate. We can see that there exist $M = N$ modes in the first propagating band, while we found $M = N - 1$ modes for the second propagating band. When looses are introduced in the system the transmission is reduced. The absorption, as shown in Fig. 4.30 (bottom), results in peaks located at each resonance mode of the system. As the number of resonating elements is increased the absorption coefficient becomes higher and broad in frequency, but only propagating modes can be efficiently absorbed.

4.5 Conclusions

The transfer matrix method is a simple but powerful analytical method for the prediction of the propagation of acoustic waves that can be used to model a broad range of one-dimensional problems. In this chapter, we have presented the method in a general way, and summarized the most common building blocks to solve one-dimensional systems in Acoustics. We have included layers of fluid and porous media, ducts and waveguides of different geometries including thermoviscous losses, locally reacting elements as Helmholtz or quarter-wavelength resonators, viscoelastic plates and membranes, or micro-perforated panels.

Through the presented examples, we have reviewed the basic applications of the method to evaluate the scattering properties of acoustic structures of particular interest. These include multi-layered porous absorbers for room acoustics, the transmission problem in double-leaf wall for building acoustics, and the analysis of the dispersion of acoustic waves in periodic media and metamaterials using locally resonant elements. Using the generalized framework provided by the transfer matrix method, many one-dimensional wave-motion phenomena as reflection, transmission, absorption, attenuation and dispersion can be studied, as illustrated in the examples of this chapter. One of the most interesting features of the TMM is that it provides fast calculations of one-dimensional structures, allowing fast and robust optimization procedures. In summary, the TMM allows the modelling of complex materials and structures using a simple theoretical framework.

Acknowledgements The authors would like to thank Julien Leng for his useful comments. N.J. acknowledges financial support from Spanish Ministry through grant "Juan de la Cierva - Incorporación" program (IJC2018-037897-I). We acknowledge support from the Metaudible (ANR-ANR-13-BS09-003) and Metaroom (ANR-18-CE08-0021) projects.

4.6 Appendix—End Corrections

Radiation corrections must be applied when there exist discontinuities in the waveguides due to a change of section. The radiation correction of a waveguide segment due to cross-section changes, $\mathbf{M}_{\Delta l}$, is modelled by a *in-series* transfer matrix as

$$\mathbf{M}_{\Delta l} = \begin{bmatrix} 1 & Z_{\Delta l} \\ 0 & 1 \end{bmatrix}, \tag{4.176}$$

where $Z_{\Delta l} = -i\omega\rho\Delta l$ is the characteristic radiation impedance and Δl is the end-correction length that depends on the geometry of the discontinuity. Below we summarize some examples.

4.6.1 Change of Section in a Waveguide

When a discontinuity is caused by a change of section in a waveguide, as those produced between the ducts that conform the neck and the cavity of a Helmholtz resonator, the length correction, Δl, is approximated by [49],

$$\Delta l = 0.82\left[1 - 1.35\frac{r_n}{r_c} + 0.31\left(\frac{r_n}{r_c}\right)^3\right] r_n. \tag{4.177}$$

where r_n is the radius of the narrower waveguide, e.g., the neck, and r_c is the radius of the wider waveguide, e.g., the cavity of a cylindrical Helmholtz resonator.

4.6.2 Side Branch

Another kind of discontinuity arises when a duct is loaded in parallel to a principal waveguide, e.g., as the one shown in Fig. 4.11. The length of the end correction Δl is given by [50]

$$\Delta l = 0.82\left[1 - 0.235\frac{r_n}{r_s} - 1.32\left(\frac{r_n}{r_t}\right)^2 + 1.54\left(\frac{r_n}{r_t}\right)^3 - 0.86\left(\frac{r_n}{r_t}\right)^4\right] r_n, \tag{4.178}$$

where r_n is the radius of the loaded waveguide and r_t is the radius of the main waveguide. This correction only depends on the radius of the waveguides, so it becomes important when the length of the duct is comparable to its radius.

4.6.3 Periodic Array of Slits

Another kind of end correction comes from the radiation from a series of slits to the free media, as occurs in slotted panels. The radiation correction for a periodic distribution of slits can be expressed as [62].

$$\Delta l = h\phi_t \sum_{n=1}^{\infty} \frac{\sin^2(n\pi\phi_t)}{(n\pi\phi_t)^3}. \tag{4.179}$$

where h is the height of the slit, $\phi_t = h/d$ and d is the distance between slits. For $0.1 \leq \phi_t \leq 0.7$ this expression reduces to

$$\Delta l_{\text{slit}} \approx -\sqrt{2}\ln\left[\sin\left(\pi\phi_t/2\right)\right]/\pi. \tag{4.180}$$

Note that, while these end corrections are good approximations, to accurately model the radiation all Bloch waves must be calculated, e.g., using modal expansion methods [27].

References

1. P.M. Morse, K.U. Ingard, *Theoretical Acoustics* (Princeton University Press, 1986)
2. J. Allard, N. Atalla, *Propagation of Sound in Porous Media: Modelling Sound Absorbing Materials 2e* (Wiley, 2009)
3. J.S. Bolton, R.J. Yun, J. Pope, D. Apfel, Development of a new sound transmission test for automotive sealant materials, in *SAE transactions*, pp. 2651–2658 (1997)
4. B.H. Song, J.S. Bolton, A transfer-matrix approach for estimating the characteristic impedance and wave numbers of limp and rigid porous materials. J. Acoust. Soc. Am. **107**(3), 1131–1152 (2000)
5. T. Lung, A. Doige, A time-averaging transient testing method for acoustic properties of piping systems and mufflers with flow. J. Acoust. Soc. Am. **73**(3), 867–876 (1983)
6. K. Peat, A transfer matrix for an absorption silencer element. Journal of Sound Vibration **146**, 353–360 (1991)
7. W.T. Thomson, Transmission of elastic waves through a stratified solid medium. J. Appl. Phys. **21**(2), 89–93 (1950)
8. W. Lauriks, P. Mees, J.F. Allard, The acoustic transmission through layered systems. J. Sound Vib. **155**(1), 125–132 (1992)
9. M. Munjal, Response of a multi-layered infinite plate to an oblique plane wave by means of transfer matrices. J. Sound Vib. **162**(2), 333–343 (1993)
10. B. Brouard, D. Lafarge, J.-F. Allard, A general method of modelling sound propagation in layered media. J. Sound Vib. **183**(1), 129–142 (1995)
11. J. Bolton, N.-M. Shiau, Y. Kang, Sound transmission through multi-panel structures lined with elastic porous materials. J. Sound Vib. **191**(3), 317–347 (1996)
12. N. Jiménez, V. Romero-García, J.-P. Groby, Perfect absorption of sound by rigidly-backed high-porous materials. Acta Acust. Acust. **104**(3), 396–409 (2018)
13. N. Jiménez, V. Romero-García, A. Cebrecos, R. Picó, V.J. Sánchez-Morcillo, L.M. García-Raffi, Broadband quasi perfect absorption using chirped multi-layer porous materials. AIP Adv. **6**(12), 121605 (2016)
14. D. Johnston, D.K. Longmore, J.E. Drew, A technique for the measurement of the transfer matrix characteristics of two-port hydraulic components, in *ASME International Congress & Exposition* (1994)
15. A. Arnau, *Piezoelectric Transducers and Applications* (Springer, 2004)
16. S. Jiménez-Gambín, N. Jiménez, J.M. Benlloch, F. Camarena, Holograms to focus arbitrary ultrasonic fields through the skull. Phys. Rev. Appl. **12**(1), 014016 (2019)
17. ASTM E2611-09, Standard test method for measurement of normal incidence sound transmission of acoustical materials based on the transfer matrix method (2009). ASTME2611

18. M. Born, E. Wolf, *Principles of Optics: Electromagnetic Theory of Propagation, Interference and Diffraction of Light* (Elsevier, 2013)
19. B. Harbecke, Coherent and incoherent reflection and transmission of multilayer structures. Appl. Phys. B **39**(3), 165–170 (1986)
20. D. Whittaker, I. Culshaw, Scattering-matrix treatment of patterned multilayer photonic structures. Phys. Rev. B **60**(4), 2610 (1999)
21. D. Torrent, J. Sánchez-Dehesa, Acoustic resonances in two-dimensional radial sonic crystal shells. New J. Phys. **12**(7), 073034 (2010)
22. P. King, T. Cox, Acoustic band gaps in periodically and quasiperiodically modulated waveguides. J. Appl. Phys. **102**(1), 014902 (2007)
23. X. Zhu, K. Li, P. Zhang, J. Zhu, J. Zhang, C. Tian, S. Liu, Implementation of dispersion-free slow acoustic wave propagation and phase engineering with helical-structured metamaterials. Nat. Commun. **7**, 11731 (2016)
24. J. Li, L. Fok, X. Yin, G. Bartal, X. Zhang, Experimental demonstration of an acoustic magnifying hyperlens. Nat. Mater. **8**(12), 931 (2009)
25. P. Leclaire, O. Umnova, T. Dupont, R. Panneton, Acoustical properties of air-saturated porous material with periodically distributed dead-end pores. J. Acoust. Soc. Am. **137**(4), 1772–1782 (2015)
26. N. Jiménez, W. Huang, V. Romero-García, V. Pagneux, J.-P. Groby, Ultra-thin metamaterial for perfect and quasi-omnidirectional sound absorption. Appl. Phys. Lett. **109**(12), 121902 (2016)
27. N. Jiménez, V. Romero-García, V. Pagneux, J.-P. Groby, Quasiperfect absorption by subwavelength acoustic panels in transmission using accumulation of resonances due to slow sound. Phys. Rev. B **95**, 014205 (2017)
28. N. Jiménez, V. Romero-García, V. Pagneux, J.-P. Groby, Rainbow-trapping absorbers: Broadband, perfect and asymmetric sound absorption by subwavelength panels for transmission problems. Sci. Rep. **7**(1), 13595 (2017)
29. V. Romero-García, G. Theocharis, O. Richoux, A. Merkel, V. Tournat, V. Pagneux, Perfect and broadband acoustic absorption by critically coupled sub-wavelength resonators. Sci. Rep. **6**, 19519 (2016)
30. A.A. Fernández-Marín, N. Jiménez, J.-P. Groby, J. Sánchez-Dehesa, V. Romero-García, Aerogel-based metasurfaces for perfect acoustic energy absorption. Appl. Phys. Lett. **115**, 061901 (2019)
31. A.D. Pierce, *Acoustics: An Introduction to Its Physical Principles and Aplications. 1989 Edition*. Acoustical Society of America, 3rd edn. (1990)
32. M.L. Munjal, *Acoustics of Ducts and Mufflers with Application to Exhaust and Ventilation System Design*. (Wiley, 1987)
33. M. Munjal, Muffler acoustics, in *Formulas of Acoustics*, pp. 689–740 (Springer, 2004)
34. Y. Kulik, Transfer matrix of conical waveguides with any geometric parameters for increased precision in computer modeling. J. Acoust. Soc. Am. **122**(5), EL179–EL184 (2007)
35. M.R. Stinson, The propagation of plane sound waves in narrow and wide circular tubes, and generalization to uniform tubes of arbitrary cross-sectional shape. J. Acoust. Soc. Am. **89**(2), 550–558 (1991)
36. M. Delany, E. Bazley, Acoustical properties of fibrous absorbent materials. Appl. Acoust. **3**(2), 105–116 (1970)
37. F. Mechel, Extension to low frequencies of the formulae of delany and bazley for a bsorbing materials. Acta Acust. Acust. **35**(3), 210–213 (1976)
38. I. Dunn, W. Davern, Calculation of acoustic impedance of multi-layer absorbers. Appl. Acoust. **19**(5), 321–334 (1986)
39. W. Qunli, Empirical relations between acoustical properties and flow resistivity of porous plastic open-cell foam. Appl. Acoust. **25**(3), 141–148 (1988)
40. Y. Miki, Acoustical properties of porous materials-modifications of delany-bazley models. J. Acoust. Soc. Jpn. (E) **11**(1), 19–24 (1990)
41. R.T. Muehleisen, C.W. Beamer IV., B.D. Tinianov, Measurements and empirical model of the acoustic properties of reticulated vitreous carbon. J. Acoust. Soc. Am. **117**(2), 536–544 (2005)

42. R. Kirby, A. Cummings, Prediction of the bulk acoustic properties of fibrous materials at low frequencies. Appl. Acoust. **56**(2), 101–125 (1999)
43. M. Garai, F. Pompoli, A simple empirical model of polyester fibre materials for acoustical applications. Appl. Acoust. **66**(12), 1383–1398 (2005)
44. D.L. Johnson, J. Koplik, R. Dashen, Theory of dynamic permeability and tortuosity in fluid-saturated porous media. J. Fluid Mech. **176**, 379–402 (1987)
45. Y. Champoux, J.-F. Allard, Dynamic tortuosity and bulk modulus in air-saturated porous media. J. Appl. Phys. **70**(4), 1975–1979 (1991)
46. T.J. Cox, P. D'antonio, *Acoustic Absorbers and Diffusers: Theory, Design and Application* (CRC Press, 2009)
47. D. Lafarge, P. Lemarinier, J.F. Allard, V. Tarnow, Dynamic compressibility of air in porous structures at audible frequencies. J. Acoust. Soc. Am. **102**(4), 1995–2006 (1997)
48. G. Theocharis, O. Richoux, V.R. García, A. Merkel, V. Tournat, Limits of slow sound propagation and transparency in lossy, locally resonant periodic structures. New J. Phys. **16**(9), 093017 (2014)
49. J. Kergomard, A. Garcia, Simple discontinuities in acoustic waveguides at low frequencies: critical analysis and formulae. J. Sound Vib. **114**(3), 465–479 (1987)
50. V. Dubos, J. Kergomard, A. Khettabi, J.-P. Dalmont, D. Keefe, C. Nederveen, Theory of sound propagation in a duct with a branched tube using modal decomposition. Acta Acust. Acust. **85**(2), 153–169 (1999)
51. D.-Y. Maa, Potential of microperforated panel absorber. J. Acoust. Soc. Am. **104**(5), 2861–2866 (1998)
52. P. Cobo, F. Simón, Multiple-layer microperforated panels as sound absorbers in buildings: A review. Buildings **9**(2), 53 (2019)
53. Z. Skvor, Vibrating systems and their equivalent circuits. Stud. Electr. Electron. Eng. **40**, 11–241 (1991)
54. F. Bongard, H. Lissek, J.R. Mosig, Acoustic transmission line metamaterial with negative/zero/positive refractive index. Phys. Rev. B **82**(9), 094306 (2010)
55. C.-C. Sung, J. Jan, The response of and sound power radiated by a clamped rectangular plate. J. Sound Vib. **207**(3), 301–317 (1997)
56. D.E. Muller, A method for solving algebraic equations using an automatic computer. Mathematical tables and other aids to computation **10**(56), 208–215 (1956)
57. T.-Y. Huang, C. Shen, Y. Jing, On the evaluation of effective density for plate-and membrane-type acoustic metamaterials without mass attached. J. Acoust. Soc. Am. **140**(2), 908–916 (2016)
58. ISO 354:2003, Acoustics-measurement of sound absorption in a reverberation room (2003)
59. Y. Makita, T. Hidaka, Comparison between reverberant and random incident sound absorption coefficients of a homogeneous and isotropic sound absorbing porous material-experimental examination of the validity of the revised $\cos\theta$ law. Acta Acust. Acust. **66**(4), 214–220 (1988)
60. T.E. Vigran, *Building Acoustics* (CRC Press, 2014)
61. ASTM E90-09, Standard test method for laboratory measurement of airborne sound transmission loss of building partitions and elements (2016)
62. F.P. Mechel, *Formulas of Acoustics*, 2nd edn. (Springer Science & Business Media, 2008)